# Boosting the toolbox for live imaging of translation

Maelle Bellec[1,2], Ruoyu Chen[3,5], Jana Dhayni[6], Cyril Favard[4], Antonello Trullo[1], Helene Lenden-Hasse[1], Ruth Lehmann[5], Edouard Bertrand[6], Mounia Lagha[1], Jeremy Dufourt[*1,4]

**Affiliations**

[1]Institut de Génétique Moléculaire de Montpellier, Univ Montpellier, CNRS, Montpellier, France.
[2]Current address: Department of Developmental Genetics, Max Planck Institute for Heart and Lung Research, Bad Nauheim, Germany.
[3]Vilcek Institute of Graduate Studies, NYU School of Medicine, New York, United States.
[4]Current address: Institut de Recherche en Infectiologie de Montpellier, CNRS UMR 9004, University of Montpellier, 1919 Route de Mende, Montpellier, 34293, Cedex 5, France.
[5]Whitehead Institute for Biomedical Research and Department of Biology, Massachusetts Institute of Technology, Cambridge, MA, USA.
[6]Institut de Génétique Humaine, University of Montpellier, CNRS, 34396 Montpellier, France.

* Correspondence to: jeremy.dufourt@irim.cnrs.fr

**Abstract:**
Live imaging of translation based on a tag recognition by a single chain antibody is a powerful technique to assess the fine tuning of translation regulation in living cells. However, especially in a multicellular organism, this approach is challenging and requires optimization in terms of expression level and detection sensitivity of the system. Here, we improved existing fluorescent tools and developed new ones to image and quantify nascent translation in the living *Drosophila* embryo and in mammalian cells. We tested and characterized five different Green Fluorescent Protein variants fused to the single chain fragment variable (scFv) and uncover photobleaching, aggregation and intensity disparities. Using different strengths of germline and somatic drivers, we determined that the availability of the scFv is critical in order to detect translation throughout development. Finally, we introduced a new translation imaging method, based on a nanobody/tag system, named ALFA_array, allowing the sensitive and simultaneous detection of the translation of several distinct mRNA species.

**Introduction:**
During development, multipotent cells progressively acquire specific fates leading to the formation of a variety of tissues. This process relies on a spatio-temporally regulated gene expression program, contributing to the reliability and reproducibility of gene expression patterns to generate the final body plan. In that process, the regulation of mRNA translation is a key step since the dynamics of translation in space and time critically affects the outcome of gene expression. Most approaches to study the regulation of translation in whole organisms rely on a bulk population of cells with poor spatial and temporal information. Consequently, the heterogeneity in the regulation of translation at the cellular and molecular level remains poorly investigated. Live imaging methods of translation have been developed in cultured cells[1–5] since 2016 and recently introduced in *Drosophila*[6–8]. These methods are based on the fluorescent labeling of nascent peptide chains. The labeling system is made of two components, a genetically-encoded antibody such as a single-chain variable fragment antibody (scFv) or Fab fragment[9–11] fused to a fluorescent protein (FP; referred to as the detector), and a N-terminal peptide epitope inserted in multiple copies in frame with the gene of interest[12]. These live imaging approaches made it possible to visualize translation up to the single-molecule scale in cultured cells but also in an entire organism[7,8]. Such technological breakthroughs provided important insights in our understanding of gene regulation through translation and, for instance, revealed the existence of motor-driven polysome transport and a spatial heterogeneity of translation at the subcellular level[5,7,13–17].

The discovery of the *Aequorea victoria* green-fluorescent protein[18,19] and especially its optimized version mEGFP[20] have revolutionized imaging of biological processes[21]. Since then, several new FPs have been and continue to be discovered and engineered[22,23]. The constant race for better FPs generally implies the optimization for fast folding, pH resistance as well as improvement of photo-physics[24].

Introduction of the bacteriophage-derived MS2 RNA binding sites, which are recognized by MS2 Coat Protein (MCP) fused to FP, provided a technique to visualize transcription in living cell. This technological advance has been subjected to numerous improvements from its initial development in 1998[25]. These improvements include increased sensitivity down to single molecules[26], implementation in a living organism[27], the generation of new stem loops to visualize single mRNAs at a high temporal resolution[28,29], artefact-free RNA[30] and double mRNA species imaging with an orthologous system[31]. However, several limitations exist with the present tools that hinder quantitative imaging. For example, protein aggregation has been observed for some systems derived from MS2 Coat Protein fused to GFP[32–34] and for scFv fused to specific GFP variants[35]. Furthermore, the expression level of the detector is critical to ensure accurate detection, particularly for translation, as most of the time one mRNA undergoes multiple rounds of translation. However, no such optimization has been made for the SunTag system in the context of a developing organism, although photo-physical properties of molecules can be variable between different systems (i.e. *in vitro* experiments, cell culture, tissues, organisms…)[24,36,37].

We tested five different GFP variants for their brightness, photobleaching and propensity to aggregation in fixed and live embryos. We also generated inducible scFv-FP constructs that, when combined with different drivers to extend the use of the SunTag system to a wider range of genes and biological questions. Furthermore, we developed an orthologous method, called ALFA-array, to visualize nascent translation in *Drosophila* embryo and mammalian cells. This system is based on a small and soluble nanobody and we show its usefulness by combining it with the SunTag to visualize translation of two different mRNA species in *Drosophila* embryos.

**Results:**

**New fluorescent protein fused to scFv to detect nascent translation.**

The SunTag method is a bipartite system based on an antibody-derived single chain variable fragment (scFv) detector fused to a fluorescent protein (FP; the detector) which binds a peptide named Supernova Tag (suntag) derived from the yeast GCN4 protein and are experimentally fused in multiple copies at the N-terminus of the gene of interest[35] (Figure 1A). To improve the system, we created new scFvs with different green fluorescent proteins under the control of *nanos* (*nos*) enhancer-promoter (EPr). This EPr drives expression in the *Drosophila* germline[38–41] allowing the maternal deposition of mature scFv-FP into the laid eggs (Figure S1A). We generated a set of four different constructs, in addition to the previously published scFv fused to the superfolder GFP (sfGFP)[42], named scFv-sfGFP[29]. The new generation of green fluorescent protein variants includes: i) the monomeric superfolder GFP2 (msGFP2)[43], ii) the mGreenLantern (GL)[44], iii) mNeonGreen[45] and iv) the monomeric *A. victoria* fluorescent protein 1 (mAvic1)[22] (Figure 1B, upper panel). Live imaging of these five scFv-FPs during embryonic development until the end of nuclear cycle 14 (n.c. 14) showed that all the scFv-FPs are well expressed, localize mainly in the nucleus, due to the presence of a nuclear localization signal, and do not form aggregates (Figure S1B and Movie S1-5). Quantification of the fluorescent intensity during the first forty minutes of n.c.14, showed that the apparent brightness of these four new scFv was similar to the scFv-sfGFP, while scFv-mAvic1 harbors a brighter signal (Figure S1C). Although, we observed that scFv-GL is prone to photobleaching (Figure S1C). We confirmed that the distribution of scFv-FP was homogenous in the embryo and

102 dots/aggregates were not detected by light-sheet imaging of the two brightest scFv-FPs, scFv-
103 mAvic1 and scFv-msGFP2 (Figure S1D and Movie S6-7).
104 We next tested the capacity of these new scFv-FPs to detect mRNA in translation in
105 embryos. We crossed the different scFv-FP lines into the background of a *twist* gene
106 endogenously tagged with MS2 and suntag (*twi_suntag_MS2_CRISPR*) (Figure 1B, lower
107 panel) and performed single-molecule Fluorescent *in situ* Hybridization (smFISH) on fixed
108 embryos to detect the tagged mRNAs. Actively translated mRNAs (polysomes) were then
109 visualized as co-localized GFP and mRNA spots. Imaging the border of *twist* mRNA
110 transcription pattern showed that the translation signal was present only in the described pattern
111 of *twist* expression (mesoderm)[46] (Figure 1C), supporting that the signal is specific. For all scFv-
112 FPs we observed a clear colocalization between mRNA (red signal) and polysomes (green
113 signal) in addition to mRNA that were not in translation (Figure S1E). Notably, a fainter signal
114 was detected for polysomes with scFv-mAvic1 and scFv-NG at this stage of embryogenesis,
115 suggesting that mAvic1 and NG are less bright or more sensitive to the fixation/smFISH
116 protocol. Immuno-smFISH with an antibody against GFP did not improve the signal but
117 increased the background. Moreover, we found that staining with only a secondary antibody
118 could label nascent foci of translation, and only when the scFv-FP is present (Figure S2A). This
119 result suggests that secondary antibodies can bind scFv-FP unspecifically and experiments
120 using both simultaneously should be avoided. We then looked at the behavior of these scFv-
121 FPs in live embryos in presence of *twi_suntag_MS2_CRISPR*. We could observe bright green
122 fluorescent dots in movement within the mesoderm (Figure 1D, Movie S8-12). To characterize
123 the detection capacity of each FP in live embryos, we measured the mean intensity of all
124 detected spots with a high temporal resolution for 4 min during n.c. 14 (Figure 1E, Movie S8-
125 12). The translation foci detected by scFv-mAvic1 and scFv-msGFP2 showed a stronger signal
126 compared to scFv-NG, scFv-sfGFP and scFv-GL (Figure 1E). Collectively, these results show
127 that the four new scFv-FPs are able to bind nascent suntag peptides and therefore detect mRNA
128 in translation in live and fixed samples.

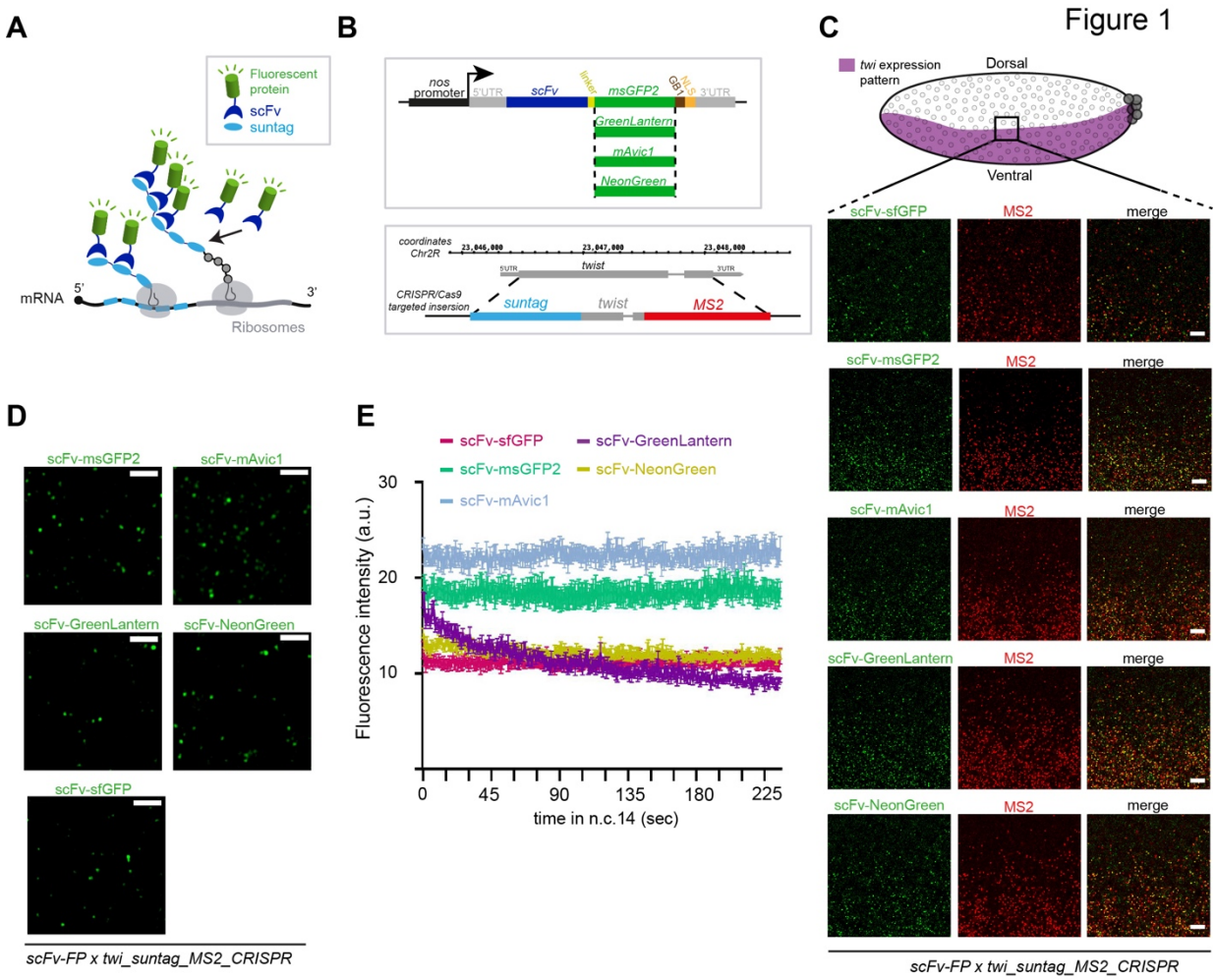


**Figure 1: Generation of different scFv-Fluorescent proteins (scFv-FP) to monitor nascent translation in *Drosophila*.**
(**A**) Schematic of the SunTag system. Once the mRNA (dark grey) is translated by the ribosomes (grey), the suntag epitopes (light blue) will be bound by the single chain variable fragment (scFv) (dark blue) fused to a fluorescent protein (FP) (green). Therefore, the nascent peptide will be detected by the accumulation of fluorescent signal. (**B**) (top) Schematic of the different constructs of scFv-FP generated in this study. scFv-msGFP2, scFv-GreenLantern, scFv-mAvic1 and scFv-NeonGreen were created for this study and scFv-sfGFP in our previous study[7]. (bottom) Schematic of the CRISPR/Cas9 targeted insertion strategy to obtain endogenous *twist* gene tagged with suntag and MS2[7]. (**C**) (top) Schematic of a sagittal view of a *Drosophila* embryo with *twi* expression pattern in purple. Anterior side is on the left, posterior on the right, dorsal on the top and ventral side on the bottom. Black square represents the imaged area of the bottom panels. (bottom) One Z-plane of confocal images from smFISH with direct fluorescent protein signal in green (scFv-msGFP2, scFv-GreenLantern, scFv-mAvic1, scFv-NeonGreen and scFv-sfGFP) and *MS2* probes (red) on *scFv-FP x twi_suntag_MS2_CRISPR* embryos in early-mid n.c. 14. Scale bar are 5µm. (**D**) Snapshots from representative fast-mode acquired confocal movies of *twi_suntag_MS2_CRISPR/+* embryos carrying either scFv-msGFP2, scFv-GreenLantern, scFv-mAvic1, scFv-NeonGreen or scFv-sfGFP proteins. Green dots represent nascent translation of *twi*. Scale bars are 5µm. (See related Movies S8-12). (**E**) Quantification across time during n.c. 14 of different scFv-FP signals from movies represented in (d), n=5 movies from at least 3 embryos for each scFv-FP. Error bars represent SEM.

## New scFv-FP prevents aggregates formation

To show whether scFv-FPs expressed under the maternal *nos* EPr could detect translation during embryogenesis, at least until gastrulation, we imaged fixed embryos at the gastrulation stage. We observed tagged Twist protein localized to nuclei in the ventral gastrulation furrow region, consistent with Twist being a mesodermal transcription factor (Figure S2B, upper panel). To test, whether the presence of a NLS in the scFv-FP construct might be responsible

155 for this nuclear localization, we imaged the localization of the Insulin-like peptide 4 (Ilp4), an
156 excreted protein expressed in the mesoderm[47]. We used the tagged Ilp4 with suntag and
157 observed scFv containing the NLS in the cytoplasm (Figure S2B, lower panel). Thus, the
158 presence of a NLS in the scFv-FP construct appears not to significantly interfere with the native
159 localization of tagged proteins.
160 Strikingly, at the gastrulation stage, bright GFP spots were observed only when using scFv-
161 sfGFP in *twi_suntag_MS2_CRISPR* embryos but not with the other scFv-FPs (Figure S3A). As
162 only the FP sequences is different between these constructs, this discrepancy might be due to a
163 difference in protein stability, scFv-sfGFP being more stable than the other variants, or that
164 scFv-sfGFP being more prone to aggregation. To decipher between these hypotheses, we used
165 smFISH to label *twi_suntag_MS2_CRISPR* mRNA in the presence of the different scFv-FPs to
166 determine whether the bright GFP spots observed during gastrulation co-localize with mRNA
167 and represent translation spots. With scFv-sfGFP we saw large green spots that were not co-
168 localized with mRNA (Figure S3B upper left panels, white arrowhead). We did not observe
169 these large spots with the any of the four new scFv-FPs (Figure S3B) suggesting an aggregation
170 of the scFv-sfGFP in the *Drosophila* embryo at the gastrulation stage in presence of
171 *twi_suntag_MS2_CRISPR*.
172 We next asked whether aggregation formation is specific to the tagged *twi* in developing
173 embryos or could also occur in cultured cells with a different suntag construct. We expressed
174 scFv-sfGFP and scFv-msGFP2 in *Drosophila* S2R+ cells along with a SunTag-luciferase
175 reporter (SunTagRLuc-MS2) (see methods, Figure S3C). The SunTagRLuc-MS2 plasmid (see
176 methods) was co-transfected with an scFv-FP plasmid as well as an MCP-Halotag plasmid (see
177 methods) to track single mRNA molecules and their translation during live-cell imaging. As
178 expected, scFv-FPs were able to label polysomes by forming GFP foci co-localizing with
179 mRNA (Figure S3D). With the scFv-sfGFP, however, we frequently observed GFP aggregates
180 which were not associated with mRNA. These aggregates were morphologically distinct from
181 translating foci and were more abundant and bigger than the GFP aggregates observed in
182 gastrulating embryos (Figure S3D-E). This result suggests an aggregation of the SunTag
183 peptides bound by the scFv-sfGFP after being translated and released from polysomes.
184 Although few aggregates were also present in cells expressing scFv-msGFP2 with the
185 SunTagRLuc-MS2 reporter (Figure S3D) this occurred with a significantly lower frequency
186 (~55% of cells without aggregates compared to ~15%) and smaller aggregate size, suggesting
187 that msGFP2 is less prone to aggregate formation.
188 These results support that the scFv-FPs containing newer generation FPs are more suitable for
189 translation analysis, as they are less likely to form aggregates.
190
191 **Monitoring translational arrest during *Drosophila* embryogenesis**
192 The low amount of translation spots observed during gastrulation suggested that *twi* translation
193 maybe have ceased at this stage of development (Figure S3A-B). However, a *twist* mRNA
194 translational arrest had not been described previously. This unexpected observation led us to
195 investigate whether *twi* transcripts were undergoing a translational arrest during n.c.14 (Figure
196 2A) using the four new scFv-FPs. Interestingly, we found at mid-late n.c. 14 (Figure 2A) that
197 the *twi_suntag_MS2_CRISPR* RNA was mostly translated at the border of the mesoderm
198 (Figure 2B and S4A-C). In comparison, polysomes dots in the center of the mesoderm were
199 less intense suggesting reduced translation (Figure 2B and S4A-C). A translational arrest was
200 recently described for *Hunchback* (*Hb*) using the SunTag system in the *Drosophila* embryo[48].
201 In this study the authors showed that after being translated in the entire Hb domain (anterior
202 half of the embryo), *hb* translation became restricted to the border of its expression pattern,
203 similarly to what we observed for *twist*. At least two models can explain this result: i) *twi*
204 translation is actively repressed at first in regions where the RNA and protein expression is

highest (as suggested for *hb*[48]) or ii) the amount of scFv-FP becomes limiting during mid-late n.c. 14 at first in regions where the RNA and protein expression is highest and prevents the detection of translation (Figure 2C upper panel). To test these hypotheses, we used the *twi_suntag_transgene*, which exhibits a stochastic expression pattern, belated transcriptional activation[29] and thus lower mRNA level compared to *twi_suntag_MS2_CRISPR.* If *twi* translation is actively repressed, a similar translational arrest should be observed for the *twi_suntag_transgene*. If the amount of scFv-FP is limiting, its translation spots should be detectable over a longer period of time (Figure 2C). Using live imaging, we observed translation spots of the *twi-suntag_transgene* at a stage when *twi_suntag_MS2_CRISPR* translation spots vanished (Figure 2D, S4D and Movie S13-15). The translation dots of the *twi_suntag_transgene* colocalized with mRNA dots in late n.c. 14 and gastrulation stage as confirmed with smFISH (Figure S4E). This result suggests that the scFv-FP amount might be limiting given the high amount of available mRNA templates when *twi* is monitored from its endogenous locus (*twi_suntag_MS2_CRISPR* allele)*,* causing a seeming translational arrest at gastrulation.

We next used an antibody against the suntag peptides (anti-GCN4) in the absence of scFv-FP and saw translation of *twi_suntag_MS2_CRISPR* mRNAs at mid-late n.c. 14 and gastrulation stage (Figure 2E and S4F). Moreover, its translation was homogenous inside the pattern of *twi* expression (Figure 2E). Altogether these results demonstrate that there is no translational arrest of *twi* mRNAs during n.c.14. Instead, the amount of scFv-FP expressed under the maternally active *nos* EPr becomes insufficient to detect translation during gastrulation, when a large pool of mRNAs is translated. Our experiments suggest that anti-GCN4 antibodies should be used as a control to distinguish between true endogenous regulation of translation and mere experimentally-dependent depletion of the labelling reagent.

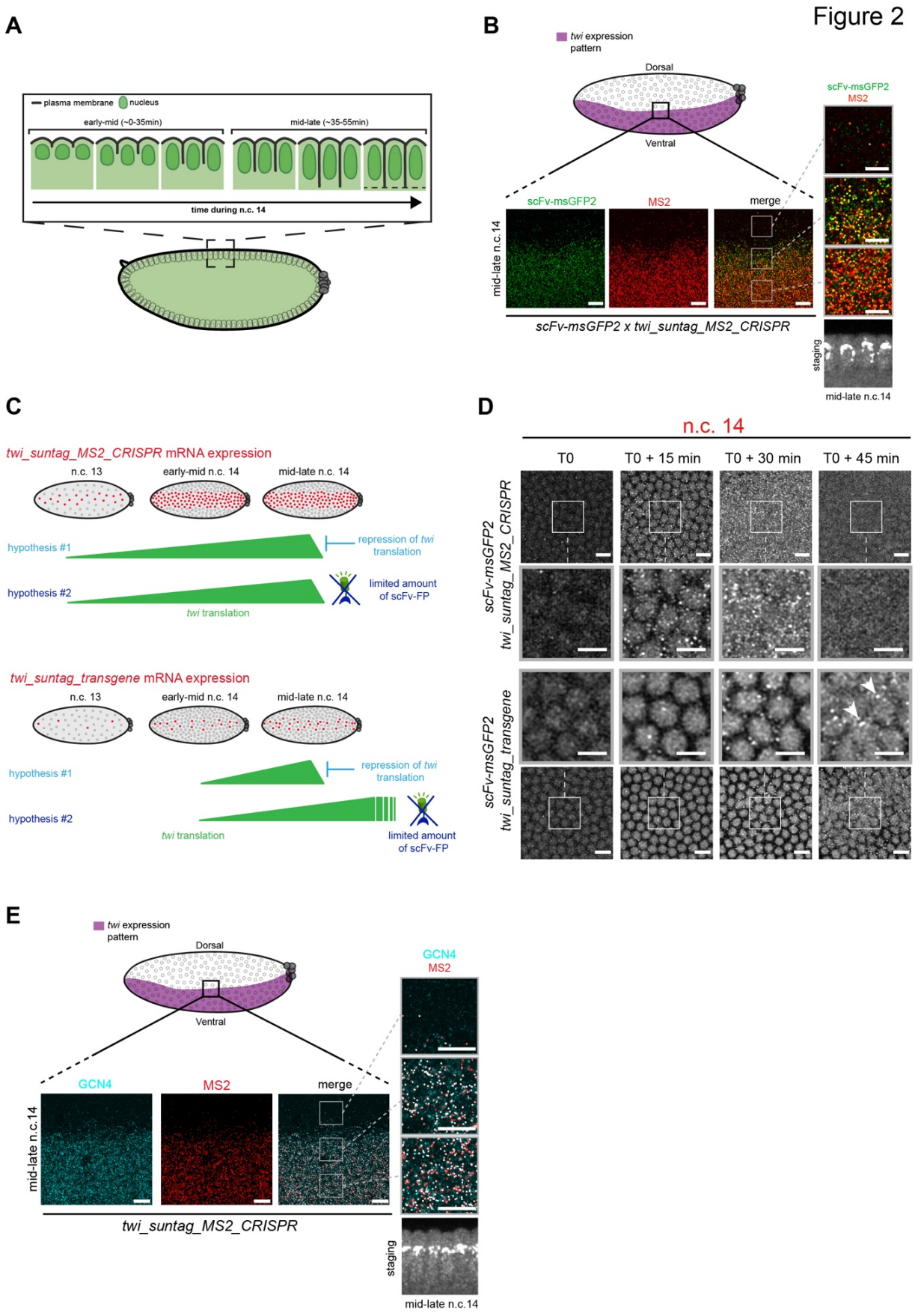


**Figure 2: scFv-FP concentration under *nos* EPr creates an artefactual translation arrest of endogenous *twi* mRNA during early embryogenesis**

(**A**) Schematic of nuclear elongation and cellularization during n.c. 14. In this study, we defined one early-mid stage (corresponding to 0 to 35min of the n.c. 14 from the mitosis) and one mid-late stage (corresponding to 35 to 55min of the n.c. 14 from the mitosis). (**B**) (top) Schematic of a sagittal view of a *Drosophila* embryo with *twi* expression pattern in purple. Anterior side is on the left, posterior on the right, dorsal on the top and ventral side on the bottom. Black square represents the imaged area of the bottom panels. (bottom) A single Z-plane of confocal images from smFISH with direct fluorescent protein signal in green (scFv-msGFP2) and *MS2* probes (red) on *scFv-msGFP2 x twi_suntag_MS2_CRISPR* embryos at mid-late n.c. 14. Gray squares represent the zoomed images in the right panels. The three different zoomed images represent external (top), border (middle) and internal (bottom) zone of the imaged pattern. Scale bars are 10µm on the larger images, and 5µm on the zoomed images. Staging is given by DAPI staining on a sagittal view of the imaged embryo (black and white image at the bottom). (**C**) Schematic representing *twi_suntag_MS2_CRISPR* mRNA expression from n.c. 13 to late n.c. 14 in red. From the observations on *twi* CRISPR translation (b), two hypotheses can be considered. Hypothesis 1 is that the decrease of translation observed at mid-late n.c. 14 is due to an active repression of translation. Hypothesis 2 is that the amount of scFv-FP becomes limiting at mid-late n.c. 14, leading to an arrest of the detected green signal. These two hypotheses are represented in the context of *twi_suntag_MS2_CRISPR* expression (above) and *twi_suntag_transgene* expression (below). *twi_suntag_transgene* mRNA is expressed more stochastically and later than *twi_suntag_MS2_CRISPR* mRNA. In hypothesis 1, a decrease of translation should be simultaneously observed for the two constructs (mid-late n.c. 14). In hypothesis 2, no arrest of translation should be observed with *twi_suntag_transgene* as the amount of mRNA is lower. (**D**) Snapshots each 15 minutes from movies of *scFv-msGFP2 x twi_suntag_MS2_CRISPR* or *scFv-msGFP2 x twi_suntag_transgene* embryos on the ventral side. T0 correspond to early n.c.14. White squares represent the zoomed images in the center of the panel. Note a persistence of translation for the *twi_suntag_transgene* at T0+45min (white arrowhead), absent in *twi_suntag_MS2_CRISPR* embryos. Scale bars are 10µm on the larger images, and 5µm on the zoomed images. (See related Movies S13-14). (**E**) (top) Schematic of a sagittal view of a *Drosophila* embryo with *twi* expression pattern in purple. Anterior side is on the left, posterior on the right, dorsal on the top and ventral side on the bottom. Black square represents the imaged area of the bottom panels. (bottom) Single Z-planes of confocal images from immuno-smFISH with anti-GCN4 antibody (cyan) and MS2 probes (red) on *twi_suntag_MS2* embryos at mid-late n.c. 14. Gray squares represent the zoomed images in the right panels. The three different zoomed images represent external (top), border (middle) and internal (bottom) zone of the imaged pattern. Scale bars are 10µm on the larger images, and 5µm on the zoomed images. Staging is given by DAPI staining on a sagittal view of the imaged embryo (black and white image at the bottom).

## Inducible scFv-FP allows imaging of translation during embryogenesis

To overtake the limitation of scFv-FP amount and allow the sustained imaging of *twi* translation from egg laying to gastrulation, we used the UAS/Gal4 system to increase the expression of scFv-FP during oogenesis. We generated four lines with the different *scFv-FPs* downstream of a *UASp* promoter (Figure 3A and S5A) and crossed these with the maternal *nos-Gal4* driver (Figure 3B) to allow expression of the scFv-FPs. No aggregation and a higher scFv-FP signal were observed in live embryos (Figure S5A, Movie S16-19 and see methods). Next, we asked if using this system would allow detection of *twi* translation until late n.c. 14 and gastrulation stage. In *twi_suntag_MS2_CRISPR* embryos with maternally provided *nos-Gal4>UASp-scFv-msGFP2* we saw that *twi* mRNA was translated throughout n.c.14 (Figure 3C), even in the most ventral part of the embryo, at the center of the *twi* domain of expression (Figure 3C). However, we were not able to detect small dots of scFv-FP, most likely corresponding to individual mature proteins, probably due to the lower signal to noise ratio, because of the increased levels of *scFv-msGFP2*. We also observed translation dots at the gastrulation stage in fixed *twi_suntag_MS2_CRISPR* embryos with *nos-Gal4>UASp-scFv-msGFP2* (Figure 3D left panels) but not with *EPr-scFv-msGFP2* (Figure 3D right panels). Similar results were observed with live imaging, where *twi_suntag_MS2_CRISPR* mRNAs were translated until gastrulation with *nos-Gal4>UASp-scFv-msGFP2* (Figure 3E and Movie S20) but not with *EPr-scFv-msGFP2* or, in the control, in the absence of *twi_suntag_MS2_CRISPR* mRNAs (Figure 3E and Movie S20).

The *UASp* promoter is used to drive expression in the germline but is less efficient in the somatic tissues[49]. On the contrary, the *UASt* containing *HSP70* promoter drives expression in the somatic tissue[50]. Recently, the *UASt* promoter has been modified to obtain a promoter, called

288 *UASz*, to drive expression in both somatic and germline tissues[51]. Due to the high amount of
289 free scFv observed with the *UASp-FP* lines, we generated a new promoter derived from the
290 *UASz*, in which we removed the translational enhancer *IVS-Syn21*[51] to prevent oversaturation
291 of free scFv-FP (Figure S5B). This new promoter named *UASy* was fused to the *scFv-msGFP2*
292 and crossed with the *nos-Gal4* driver line. As all the other constructs generated in this study,
293 *nos-Gal4>UASy-scFv-msGFP2* alone does not lead to aggregates during early embryogenesis
294 (Figure S5C and Movie S21). Unfortunately, when we analyzed the translation of
295 *twi_suntag_MS2_CRISPR* mRNA at the end of n.c. 14, we observed a similar pattern - although
296 less pronounced - as with *scFv-msGFP2* where translation was mostly present at the border of
297 *twi* pattern (Figure S5D), likely due to the weaker expression of the *UASy* compared to *UASp*
298 promoters and consequent depletion of scFv in the central mesoderm. Maternal expression of
299 the scFv-FP constructs limits our ability to observe translational dynamics at later stages in
300 development. To overcome this, we crossed *UASy-scFv-msGFP2* with an early zygotic *nullo-*
301 *Gal4* driver to express throughout the embryo. This revealed scFv-msGFP2 expression at the
302 beginning of gastrulation (Movie S22) and a strong and homogeneous expression in somatic
303 tissues of later embryos (Figure S5E). We conclude that the *nos-Gal4>UASp-scFv-FP*
304 represents a good tool to image translation from early embryogenesis to gastrulation stage and
305 that the new *UASy-scFv-msGFP2* will enable the imaging of translation in somatic cells at later
306 stages.

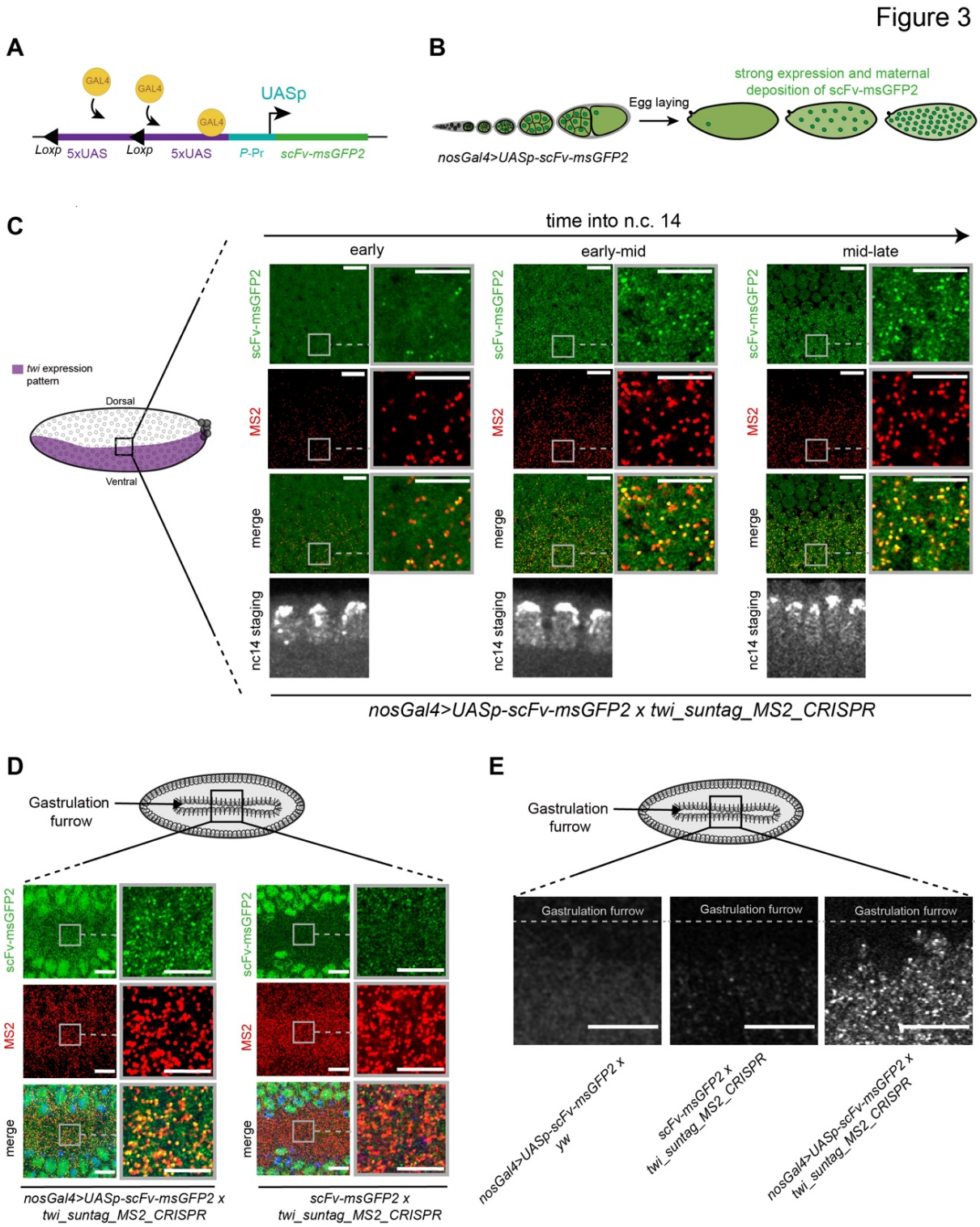


**Figure 3: Increasing scFv-FP expression allows translation detection at later stages**
(**A**) Schematic of *UASp-scFv-msGFP2* construct and activation by the Gal4 protein. 10 UAS sequences (purple) are placed upstream the P-promoter (blue) and scFv-msGFP2 (green) sequences. Gal4 proteins (yellow) will bind the UAS sequences to activate transcription of the scFv-msGFP2. (**B**) Schematic of the expression of the *scFv-msGFP2* in *nosGal4>UASp-scFv-msGFP2* female strain during oogenesis until egg deposition. (**C**) (left) Schematic of a sagittal view of a *Drosophila* embryo with *twi* expression pattern in purple. Anterior side is on the left, posterior on the right, dorsal on the top and ventral side on the bottom. Black square represents the imaged area of the right panels. Single Z-planes of confocal images from smFISH with direct scFv-msGFP2 fluorescent protein signal (green) and *MS2* probes (red) on *nosGal4>UASp-scFv-msGFP2 x twi_suntag_MS2_CRISPR*

embryos in early, early-mid and mid-late n.c. 14. Gray squares represent the zoomed images in for each panel. The three different zoomed images represent external (top), border (middle) and internal (bottom) zone of the imaged pattern. Nuclei are counterstained with DAPI (grey, bottom images) for staging. Scale bars are 10µm on the larger images, and 5µm on the zoomed images. (**D**) (top) Schematic of a *Drosophila* embryo on the ventral side with gastrulation furrow represented with invaginating cells. Black square represents the imaged area of the bottom panels. (bottom) Single Z-planes of confocal images from smFISH with direct scFv-msGFP2 fluorescent protein signal (green) and *MS2* probes (red) on *nosGal4>UASp-scFv-msGFP2 x twi_suntag_MS2_CRISPR* and *scFv-msGFP2 x twi_suntag_MS2_CRISPR* embryos at gastrulation stage and on the ventral side. Scale bars are 10µm on the larger images, and 5µm on the zoomed images. Note that translation dots are visible only with *nosGal4>UASp-scFv-msGFP2*. (**E**) (top) Schematic of a *Drosophila* embryo on the ventral side with gastrulation furrow represented with invaginating cells. Black square represents the imaged area of the bottom panels. (bottom) Single Z-planes of confocal images from movie of *scFv-msGFP2 x yw, scFv-msGFP2 x twi_suntag_MS2_CRISPR* and *nosGal4>UASp-scFv-msGFP2 x twi_suntag_MS2_CRISPR* embryos at gastrulation stage (furrow represented with grey dashed line). Scale bars are 10µm. (See related Movie S20).

## Development of the ALFA_array system to monitor translation

After having optimized scFv-FP-based detector, we sought to generate an optimized orthologous system to the SunTag to allow the detection of translation of two different RNA species. To this end, we searched for a highly specific nanobody/tag couple and decided to use the recently developed ALFA-Tag[52]. The ALFA-Tag is a small peptide that harbors several advantages: its synthetic sequence is absent from the proteome of most studied model organisms, its sequence is smaller than that of the SunTag sequence (15 amino acid compare to 19, respectively Figure 4A), it is monovalent, hydrophilic and was effective in *Drosophila* for protein manipulation[53]. Finally, the nanobody anti-ALFA detector (NB-ALFA) is smaller than the scFv (Figure 4B), is quite soluble and displays a strong binding affinity for the ALFA-Tag (measured at 26pM)[52]. Taking advantage of these properties, we multimerized the ALFA-Tag sequences to create a 12X and 32x_ALFA-array. Each ALFA-tag sequence was flanked by a proline, to reduce potential influence of neighboring secondary structures, and a spacer of 5 amino acid (GSGSG) to minimize steric hindrance of neighboring peptide binding sites (Figure 4A, C). The NB-ALFA was fused to the msGFP2 and to the GB1 solubilization tag (also used for the scFv) to avoid potential aggregation caused by the multimerization of ALFA-tag sequences. Finally, we generated a *Drosophila* line with the *NB-ALFA-msGFP2* under the control of *nos* EPr (*NB-ALFA-msGFP2)*. The system was also tested in mammalian cells (see below).

To study translation in *Drosophila* embryos using the 32x ALFA-Array system, we chose to tag the *Ilp4* gene for its small size. We reasoned that if we could visualize translation with a very short transcript/protein, it may be possible for longer ones. A 32x_ALFA-array was inserted between the *Ilp4* initiation codon and *Ilp4* gene body, appended with *Ilp4* UTRs and *Ilp4* EPr (*Ilp4_32x_ALFA-Array*, Figure 4D). With immuno-smFISH we found that the *Ilp4_32x_ALFA-Array* was expressed in the mesoderm of early *Drosophila* embryos (Figure S6A) consistent with previous reports for Ilp4[47]. The anti-ALFA formed bright dots specifically colocalizing with *Ilp4_32x_ALFA-Array* mRNAs representing foci of translation (Figure S6B-C), while the *Ilp4_32x_ALFA-Array* was not recognized by the anti-GCN4 antibody (Figure S6A).

We first confirmed by live imaging that the *NB-ALFA-msGFP2* strain is expressed during embryonic development until the end of n.c.14, that it was mainly localized to the nucleus, and that it did not form any aggregates (Figure S6D and Movie S23). The *Ilp4_32x_ALFA-Array* was crossed with *NB-ALFA*-msGFP2 and the resulting embryos showed bright GFP spots overlapping with *Ilp4_32x_ALFA-Array* mRNAs (Figure 4D), showing the ability of NB-ALFA-msGFP2 to bind 32x_ALFA-Array *in vivo.* Next, we monitored translation in live embryos and observed bright GFP dots appearing on the ventral side of the embryo (Figure 4E and Movie S24). The signal was restricted to the mesoderm during n.c.14 (Figure S6E and Movie S25) and became more restricted to the ventral furrow during gastrulation (Figure S6F

369 and Movie S25), demonstrating the specificity of the signal detection. Thus, the
370 *Ilp4_32x_ALFA-Array* - NB-ALFA-msGFP2 system is a useful alternate tool to detect mRNA
371 translation during early embryogenesis. To test if we use this system to image translation of
372 two distinct mRNA species in the same embryo, the *Ilp4_32x_ALFA-Array* was crossed with
373 the *twi_suntag_transgene* (Figure 4F). Using immuno-smFISH in n.c.14 embryos, we observed
374 the two overlapping expression patterns of Twi and Ilp4 as well as the posterior region where
375 only Twi is present (Figure S6G). With higher resolution images, we could visualize single
376 molecules of *Ilp4* mRNA in translation well distinct from *twi* mRNA translation dots (Figure
377 4G). Furthermore, we were able to distinguish the localization of Ilp4 protein in the cytoplasm
378 from Twi protein in the nucleus (Figure 4H).
379 Together, these results demonstrate that the 32x_ALFA-array can be used in conjunction with
380 the SunTag system to study translation of two different mRNAs and their protein localization
381 during early embryogenesis.
382

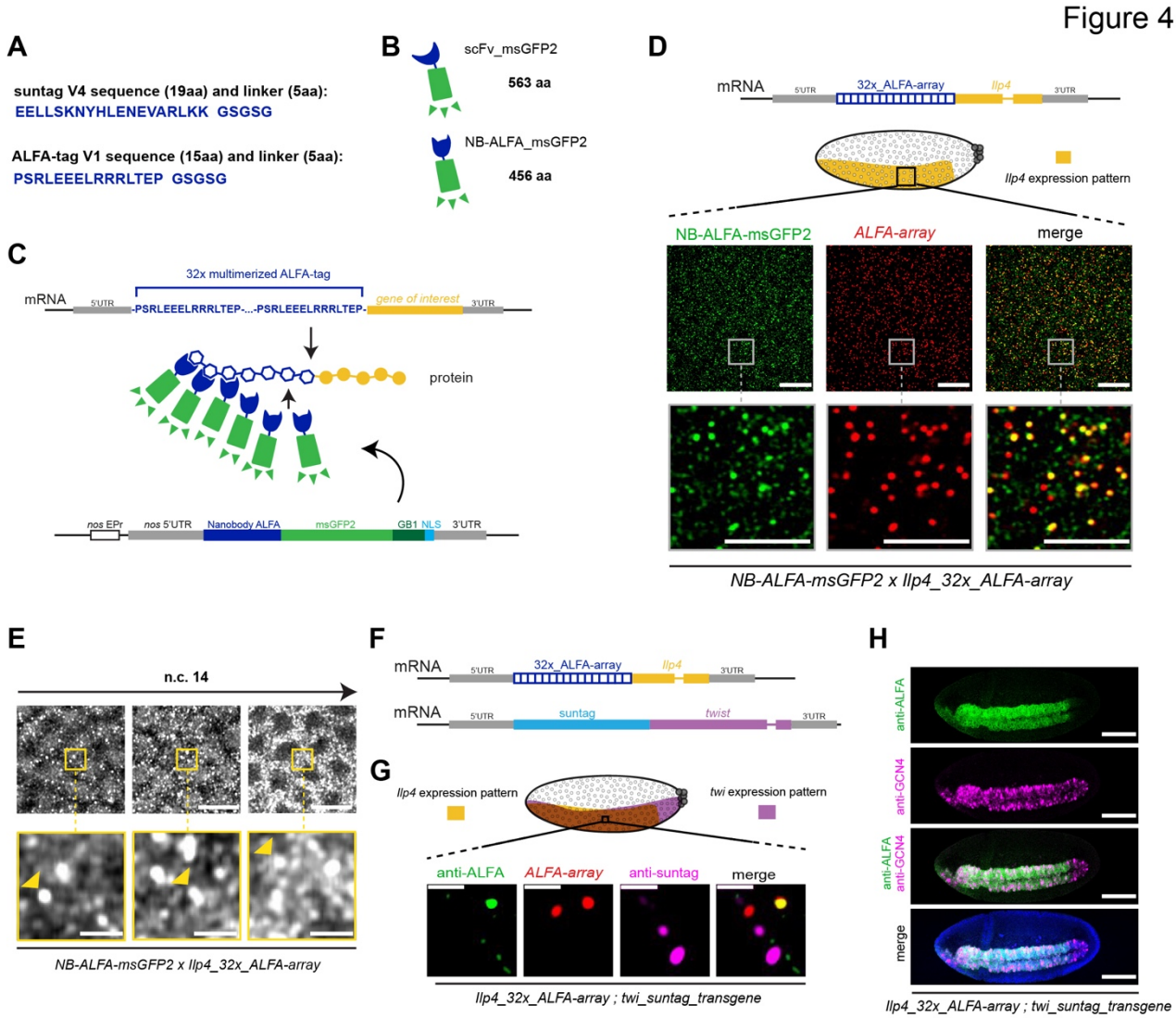


383 **Figure 4: Development of the ALFA_array system to detect nascent translation in *Drosophila***
384 (**A**) Peptide sequence of one suntag with its linker (24 amino-acids) and peptide sequence of the ALFA-tag with
385 its linker (20 amino-acids). (**B**) Schematic of the scFv and the nanobody ALFA (NB-ALFA) fused to the
386 fluorescent protein msGFP2 and their size in amino-acid (aa). (**C**) Schematic of the ALFA-array system developed
387 in this study to detect translation. 32 ALFA-tag sequences were multimerized (blue amino-acid sequence) and
388 inserted at the 5' of the gene of interest sequence (yellow). Upon translation, nanobodies ALFA fused to msGFP2
389 (NB-ALFA_msGFP2) will bind to the ALFA-tag peptides. As a bipartite system, the NB-ALFA is expressed

under *nos* EPr fused to *msGFP2*, *Streptococcal protein G* (*GB1*) domain and a *Nuclear Localisation Signal* (*NLS*). (**D**) Representation of the transgene mRNA containing 32x_ALFA-array in frame with the *insulin-like peptide 4* (*Ilp4*) gene sequence. Schematic of a sagittal view of a *Drosophila* embryo with *Ilp4* expression pattern in yellow. Anterior side is on the left, posterior on the right, dorsal on the top and ventral side on the bottom. Black square represents the imaged area of the bottom panels. One Z-plane of confocal images from smFISH with direct Nb-ALFA-msGFP2 fluorescent protein signal (green) and 32x_*ALFA-array* probes (red) on *NB-ALFA_msGFP2>Ilp4_32x_ALFA-array* embryos in early-mid n.c. 14 on the ventral side. Scale bars are 10µm on the larger images, and 5µm on the zoomed images. (**E**) Snapshots from representative fast-mode acquired confocal movies of *Ilp4_32x_ALFA-array/+* n.c. 14 embryos carrying *NB-ALFA_msGFP2*. Bright white foci represent nascent translation of *Ilp4* transgene. Yellow squares represent zoomed images of the top panels. Nascent translation of *Ilp4* transgene is indicated by yellow arrowheads. Scale bars are 10µm on the larger images, and 2µm on the zoomed images. (See related Movies S24). (**F**) Representation of the transgene mRNAs containing 32x_ALFA-array fused to *Ilp4* coding sequence or suntag fused to *twist* coding sequence used in (G) and (H). (**G**) Schematic of a *Drosophila* embryo on the ventral side with *twi* expression pattern in purple and *Ilp4* in yellow. Black square represents the imaged area of the bottom panels. One Z-plane of confocal images from immuno-smFISH with *NB-ALFA_msGFP2* (green) labeling nascent translation of *Ilp4_32x_ALFA-array*, probes against *32x_ALFA-array* (red) labeling *Ilp4_32x_ALFA-array* mRNA molecules and anti-GCN4 antibody labeling nascent translation of *twi_suntag_transgene* (magenta) in n.c. 14 embryos. Scale bars are 1µm. (**H**) Maximum intensity projection of a whole embryo confocal images from immuno-staining with anti-ALFA antibody (green) and anti-GCN4 antibody (magenta) on *Ilp4_32x_ALFA-array; twi_suntag_transgene* gastrulating embryo. Scale bars are 100µm.

To test the performance of the ALFA-tag labeling system to image translation in a different model, we turned to mammalian cells. We generated HeLa cells expressing a NB-ALFA-sfGFP recombinant nanobody and then inserted a 12xALFA-Array repetition at the N-terminus of the DYNC1H1 gene by CRISPR-mediated knock-in (Figure 5A), as previously done for the SunTag[1]. Heterozygous clones were obtained and imaged with and without a thirty-minute puromycin treatment to inhibit translation. In untreated cells, bright foci were observed in the cytoplasm, which disappeared following puromycin addition (Figure 5B). In addition, smFISH against the endogenous DYNC1H1 mRNAs revealed that the bright ALFA-tag foci colocalized with mRNA spots (Figure 5C), confirming that these correspond to DYNC1H1 polysomes. The quality of the signal obtained with only 12 repeats of the ALFA-tag demonstrates the efficiency of this labeling system to image translation.

Figure 5

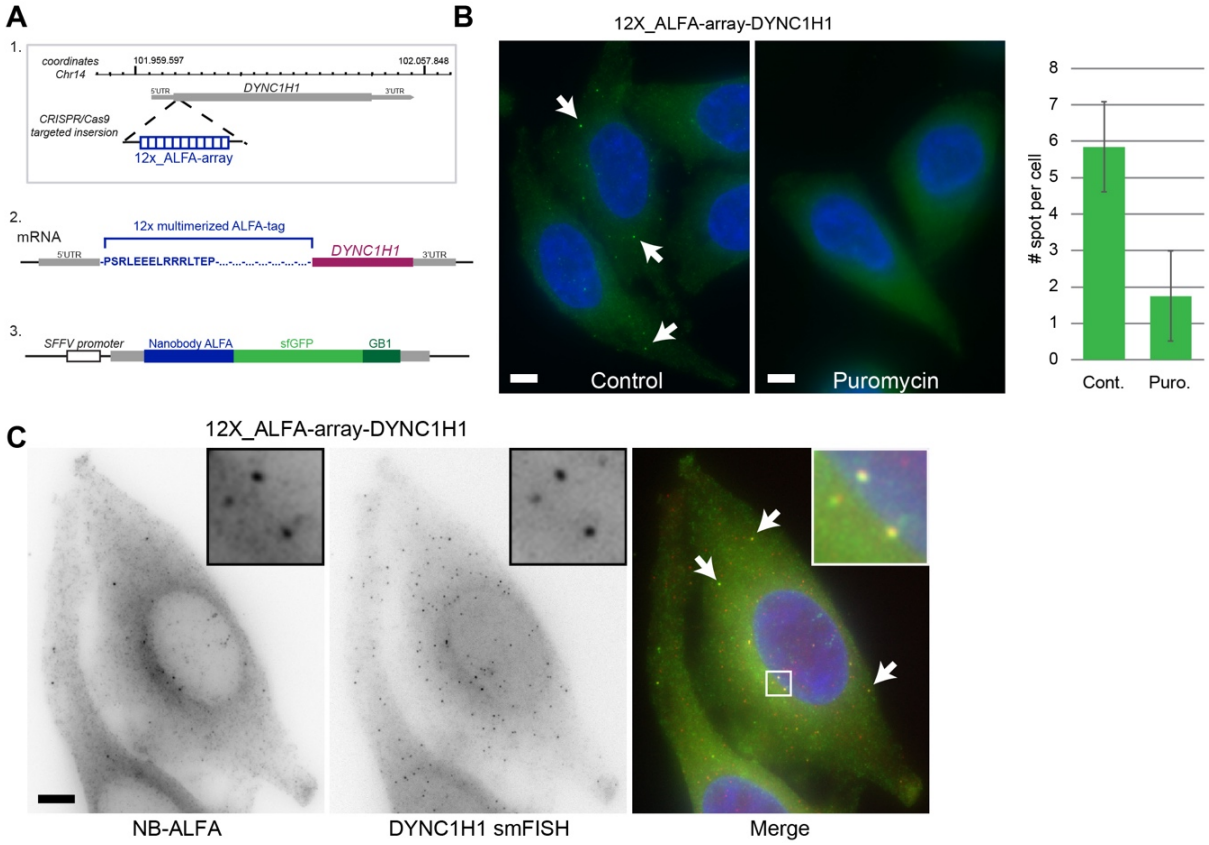


**Figure 5: Development of the ALFA_array system to detect nascent translation in mammalian cells**
(**A**) (1.) Schematic of the CRISPR/Cas9 targeted insertion strategy to obtain endogenous *DYNC1H1* gene tagged with 12X ALFA-tag. (2.) Schematic of the ALFA-array system developed in mammalian cells. 12 ALFA-tag sequences were multimerized (blue amino-acid sequence) and inserted at the 5' of the gene of interest sequence (DYNC1H1, yellow). (3.) The NB-ALFA is expressed under *spleen focus-forming virus (SFFV)* promoter fused to *sfGFP* and *Streptococcal protein G* (*GB1*) domain. (**B**) Left: micrographs of HeLa cells expressing a DYNC1H1 allele endogenously tagged 12xALFA-Array tag and NB-ALFA-sfGFP, and treated (right) or not (left) with puromycin. Green: NB-ALFA-sfGFP signal; blue: DAPI. Scale bars are 5µm. Arrows: NB-ALFA-sfGFP spots. Right: quantification of the number of NB-ALFA-sfGFP spots per cell, with and without puromycin treatment. Error bars: standard deviation (n=40 cells). (**C**) Micrographs of HeLa cells expressing a DYNC1H1 allele endogenously tagged 12xALFA-Array tag and NB-ALFA-sfGFP, and hybridized in situ with a set of probes against DYNC1H1 mRNAs. On the merged panel: NB-ALFA-sfGFP signal (green); smFISH signals (red); DAPI (blue). Scale bar is 5µm. Arrows: DYNC1H1 polysomes.

## Discussion

Amplification of biological signals is crucial to study many biological processes with a high spatio-temporal resolution and single-mRNA-molecule sensitivity. Live imaging of translation at single molecule resolution is a relatively recent technology implemented in 2016 in tissue culture and in 2021 in multicellular organisms. In this study, we provide a powerful toolbox to image translation in living cells and organisms. We will discuss some of the limitations and challenges that need to be considered to obtain robust and reliable results.

Our data show that the choice of the fluorescent protein is a key element for the signal quality of translation imaging-based systems. The development of fluorescent proteins is a very rapidly evolving field and FP-based tools need to be updated to optimize their use. Often, the choice of the FP needs to be empirically defined for each cell type, tissue or organism studied. Local translation of specific mRNAs is an important biological process to control gene expression in

space and time. To obtain quantitative answers it is necessary to precisely resolve the location of mRNAs and where their translation occurs. In the present experimental designs, with the orthologous scFv and the NB-ALFA, the use of secondary antibodies can confound signal interpretation as they appear to bind the scFv and NB-ALFA fusion. This recognition may be due to the linker and GB1 sequences added, as a recent study in plants, which used Western-blot analysis, showed a strong affinity between GB1 and IgG[54]. To combine translation imaging with immunofluorescence, a solution to this problem would be directly linking a fluorophore to a primary antibody.

An important aspect in imaging live embryos or tissues is signal amplification to increase the signal-to-noise ratio. Indeed, in systems like the MS2/MCP, llama-Tag/Fluorescent protein[55] or scFv/SunTag and their derivatives, the signal appears by local specific accumulation of fluorescent detector, over a diffuse background of molecules freely diffusing in the cells. To improve the signal-to-noise ratio, one can reduce the available free fluorescent detector and therefore the background using weak promoters or targeting the free fluorescent detector to other cellular compartments such as the nucleus, or specific organelles for cytoplasmic analysis. However, one should be careful that the availability of these fluorescent detector does not become limiting as more and more RNAs and proteins are produced during development. As we illustrate here, the available concentration of the detector can be a major challenge in developing organisms, especially when the source of the detector is controlled by an endogenous promoter and when the amount of template mRNA in translation is important. This limitation can also be particularly important when a burst of translation occurs such as during viral infection[14,15]. We provide a direct example for detector limitation during early embryogenesis. Here, early activated genes such as *twist* are highly and rapidly transcribed and translated leading to rapid depletion of free detector. We demonstrate the importance of distinguishing between detector depletion and cessation of translation by validating the results with direct immunostaining against the tag of choice. We also show that increasing the expression of the detector can overcome the detection problem but will reduce the signal-to-noise ratio and has thus to be taken into consideration for the specific experimental design. To reach conditions that can most accurately capture the dynamics of translation, diverse *UAS* promoters together with a variety of available Gal4 drivers should be tested depending on the tissue of interest and the expression level of the tagged gene.

Studies on mRNA localization and local translation have speculated that different mRNAs species may be translationally co-regulated[56–58]. To obtain independent translational readouts of different mRNA simultaneously, one can combine orthogonal tagging systems. In Boersma et al., the authors inserted the MoonTag and the SunTag[16] into different translational reading frames of the same RNA. This allowed them to observe in real time heterogeneities in the start site selection of individual ribosomes on a single mRNA molecule. Here, we introduce a new antibody-based detector/tag pair to image translation in living cells and organisms based on multimerization of the ALFA-Tag. The ALFA-array system has a number of advantages: i) it comes from synthetic design and its sequence is thus absent from most organisms; ii) the tag is small, soluble, hydrophilic and lacks aldehydes-sensitive amino acids altered by fixation; iii) the detection is made by a nanobody, which is small and soluble, and has a very strong affinity for the ALFA-Tag ($K_d$ of 27pM), which favorably compares to the MoonTag (Kd of 30 nM)[16].

The new translation imaging system described in this study should be applicable to many different organisms to follow localization and control of protein translation. Moreover, the availability of several orthogonal systems will allow to better analyze of the complexity of translation dynamics by simultaneously comparing several mRNA in diverse cellular environments and conditions. The wide range of applications of the ALFA-array system, coupled with other antibody-based translation detector, provides to the scientific community a highly versatile toolbox that will facilitate future scientific breakthroughs.

500
501
502
503
504 **Online methods**
505
506 **Reagents created in this study**

| Reagent type | Genotype | Insertion type and chromosome number | Additional information |
|---|---|---|---|
| *Drosophila* line | *nosEPr > scFv-msGFP2* | Landing site insertion vk33 – Chr. III | mini-white marker, plasmid also available (in pBPhi vector) |
| *Drosophila* line | *nosEPr > scFv-GL* | Landing site insertion vk33 – Chr. III | mini-white marker, plasmid also available (in pBPhi vector) |
| *Drosophila* line | *nosEPr > scFv-mNeonGreen* | Landing site insertion vk33 – Chr. III | mini-white marker, plasmid also available (in pBPhi vector) |
| *Drosophila* line | *nosEPr > scFv-mAvic1* | Landing site insertion vk33 – Chr. III | mini-white marker, plasmid also available (in pBPhi vector) |
| *Drosophila* line | *nosEPr > scFv-msGFP2* | Landing site insertion vk27 – Chr. II | mini-white marker, plasmid also available (in pBPhi vector) |
| *Drosophila* line | *nosEPr > scFv-GL* | Landing site insertion vk27 – Chr. II | mini-white marker, plasmid also available (in pBPhi vector) |
| *Drosophila* line | *nosEPr > scFv-mNeonGreen* | Landing site insertion vk27 – Chr. II | mini-white marker, plasmid also available (in pBPhi vector) |
| *Drosophila* line | *nosEPr > scFv-mAvic1* | Landing site insertion vk27 – Chr. II | mini-white marker, plasmid also available (in pBPhi vector) |
| *Drosophila* line | *UASp > scFv-msGFP2* | Landing site insertion vk33 – Chr. III | mini-white marker, plasmid also available (in pBPhi vector) |
| *Drosophila* line | *UASp > scFv-GL* | Landing site insertion vk33 – Chr. III | mini-white marker, plasmid also available (in pBPhi vector) |
| *Drosophila* line | *UASp > scFv-mNeonGreen* | Landing site insertion vk33 – Chr. III | mini-white marker, plasmid also available (in pBPhi vector) |

| | | | |
|---|---|---|---|
| *Drosophila* line | *UASp > scFv-mAvic1* | Landing site insertion vk33 – Chr. III | mini-white marker, plasmid also available (in pBPhi vector) |
| *Drosophila* line | *UASy > scFv-msGFP2* | Landing site insertion - vk33 Chr. III | mini-white marker, plasmid also available (in pBPhi vector) |
| *Drosophila* line | *nosEPr > NB-ALFA-msGFP2* | Landing site insertion - vk33 Chr. III | mini-white marker, plasmid also available (in pBPhi vector) |
| *Drosophila* line | *Ilp4_32x_ALFA-Array* | Landing site insertion - vk33 Chr. III | mini-white marker, plasmid also available (in pBPhi vector) |
| DNA plasmid | NB-ALFA in pUC57-Simple | N/A | Synthetized by Genescript, codon optimized |
| DNA plasmid | ALFA-Array in pUC57-Simple | N/A | Synthetized by Genescript, with linker GSGSG and codon optimized |
| DNA plasmid | pMT-SuntagRLucFKBP24MS2v5-SV40 | N/A | Used in S2 cell experiments |
| DNA plasmid | pAWF-stdMCP-stdHalotag | N/A | Used in S2 cell experiments |
| DNA plasmid | pAWF-scFv-msGFP2 | N/A | Used in S2 cell experiments |
| DNA plasmid | pAWF-scFv-sfGFP | N/A | Used in S2 cell experiments |
| DNA plasmid | 12xALFA-Array for CRISPR tagging DYNC1H1 | N/A | Used for HeLa cells experiments |
| DNA plasmid | NB-ALFA-sfGFP in pHR | N/A | Used for HeLa cells experiments |

**Fly stocks, handling and genetics**

The *yw* fly stock was used as a wild type. The germline driver *nos-Gal4:VP16* (BL4937) and the *His2av-mRFP* (Bl23651) fly stocks come from Bloomington Drosophila Stock Center. The *nullo-Gal4* fly stock comes from RL laboratory. The *twi_suntag_MS2_CRISPR* and *twi_suntag_transgene* lines were from[7]. Briefly, the 32x suntag sequence from[59] (containing thirty three suntag repeats) was inserted in frame into *twi* gene[7] and 128X MS2 from[28] placed just after the stop codon. All live experiments were done at 21 °C except when using - or comparing to - strains containing UAS-GAL4 which were done at 25 °C.

**Cloning and transgenesis**

*scFv-FP* under *nanos* enhancer-promoter (EPr) lines were generated using NEBuilder® HiFi DNA Assembly Master Mix with primers listed in supplementary table 1 and inserted into scFv-sfGFP vector[7] digested with BamHI/XhoI. The transgenic construct was inserted into the VK00033 (BL9750) and VK00027 (BL9744) landing site using PhiC31 targeted insertion[60]. *UASp-scFv-FP* lines were done by inserting fragment of the scFv-FP plasmid digested with XhoI/HpaI in the UASp-scFv-sfGFP vector[6] digested with XhoI/HpaI. The transgenic construct

524 was inserted in the VK00033 (BL9750) landing site using PhiC31 targeted insertion[60].
525 Fluorescent proteins were extracted from plasmids: mAvicFP1 from pNCST-mAvicFP1
526 (addgene 129509), mGreenLantern from pcDNA3.1-mGreenLantern (addgene 161912),
527 msGFP2 (addgene 160461), mNeonGreen is a kind gift from S.Piatti. The Ilp4 transgene
528 (regulatory regions and coding sequence) was synthesized (GenScript Biotech) into pUC57-
529 simple[7]. The 32x_ALFA_array repeats were synthesized (GenScript Biotech) into pUC57-
530 simple (see supplementary materials). The 32x_ALFA_array was inserted between Kpn1 and
531 EcoRV restriction sites of the Ilp4 puc57-simple vector. Ilp4-ALFA_array fragment was
532 inserted into pBPhi using PmeI and Nhe1 and injected into BL9750 using PhiC31 targeted
533 insertion[60] (BestGene, Inc.). All cloning for plasmids used in *Drosophila* S2 cells were
534 performed using In-Fusion® HD Cloning Plus Kit (Takara Bio) and PCR was carried out with
535 CloneAmp HiFi PCR premix (Takara Bio). Primers used are listed in supplementary table 1.
536 To inducibly express SunTag in S2 cells, we generated pMT-SuntagRLucFKBP24MS2v5-
537 SV40 by inserting SuntagRLucFKBP24MS2v5 fragment (addgene 119946) into pMT
538 backbone that was PCR-amplified from pMT-EGFPActin5C (addgene 15312) with In-Fusion®
539 HD Cloning Plus Kit. For constitutive expression in S2 cells, pAWF (DGRC stock # 1112) was
540 used as an expression vector. pAWF-stdMCP-stdHalotag was generated by inserting stdMCP-
541 stdHalotag (addgene 104999) into PCR-linearized pAWF vector using In-Fusion® HD Cloning
542 Plus Kit. To generate pAWF-scFv-FPs, sequences containing scFv fused to various fluorescent
543 proteins and GB1-NLS were amplified from *scFv-FP* under *nanos* enhancer promoter plasmids
544 generated for in this article and ligated with PCR-linearized pAWF vector using In-Fusion®
545 HD Cloning Plus Kit. All plasmid sequences are listed in supplementary materials.
546
547 **Single molecule fluorescence *in situ* hybridization (smFISH) and immuno-smFISH in**
548 ***Drosophila***
549 A pool of 0-4h after egg-laying (AEL) embryos were dechorionated with bleach for 3 min and
550 thoroughly rinsed with $H_2O$. They were fixed in 1:1 heptane:formaldehyde-10% for 25 min on
551 a shaker at 450 rpm; formaldehyde was replaced by methanol and embryos were shaken by
552 hand for 1 min. Embryos that sank to the bottom of the tube were rinsed three times with
553 methanol and kept at -20°C for further use.
554 Embryos were washed 5 min in 1:1 methanol:ethanol, rinsed twice with ethanol 100%, washed
555 5 min twice in ethanol 100%, rinsed twice in methanol, washed 5 min once in methanol, rinsed
556 twice in PBT-RNasin (PBS 1x, 0.1% tween, RNasin® Ribonuclease Inhibitors). Next, embryos
557 were washed 4 times for 15 min in PBT-RNasin supplemented with 0.5% ultrapure BSA and
558 then once 20 min in Wash Buffer (10% 20X SCC, 10% Formamide). They were then incubated
559 overnight at 37 °C in Hybridization Buffer (10% Formamide, 10% 20x SSC, 400 µg/ml *E. coli*
560 tRNA (New England Biolabs), 5% dextran sulfate, 1% vanadyl ribonucleoside complex (VRC)
561 and smFISH Stellaris probes against *suntag*[7] or 32x_ALFA_array coupled to Quasar 570
562 (supplementary table 1) or probes against 32X MS2 coupled to Cy3 (from E. Bertrand)[61] and/or
563 GCN4 primary antibody (Novus Biologicals C11L34) (1/200) and/or affinity purified rabbit
564 anti-ALFA polyclonal antibody (NanoTag Biotechnologies) (1/200). Probe sequences are listed
565 in Supplementary table 1. The next day, secondary antibody (1/500 anti-mouse Alexa 488-
566 conjugated (Life Technologies, A21202); anti-mouse Alexa 647-conjugated (Invitrogen,
567 A32728); anti-rabbit Alexa 555-conjugated (Life Technologies, A31572) or anti-rabbit Alexa
568 488-conjugated (Life Technologies, A21206)) was added if necessary, during 1h at 37° in Wash
569 Buffer. DAPI was added at 45min (1/1000). Embryos were then washed three times 15min in
570 2x SCC, 0.1% Tween at room temperature before being mounted in ProLong® Diamond
571 antifade reagent.
572 Images were acquired using a Zeiss LSM880 confocal microscope with an Airyscan detector
573 in Super Resolution (SR) mode. GFP/Alexa-488 was excited using a 488 nm laser, Cy3/ were

excited using a 561 nm laser, Alexa 670 was excited using a 633 nm laser. Laser powers were: 27µW for 488nm laser (9µW for UAS>nos images), 80µW for 561nm laser and 46µW for 640nm laser. Laser powers were taken under a 10X objective. Figures were prepared with ImageJ (National Institutes of Health), Photoshop (Adobe Systems), and Illustrator (Adobe Systems)

**Cell culture**

Drosophila S2R+ cells (DGRC Stock 150) were maintained at 25°C in Schneider's medium containing 10% Fetal Bovine Serum and 1% Penicillin-streptomycin. For the transfection, 0.7x10^6 cells in 350ul were seeded into each well of a 24-well plate. Cells are transfected with plasmid mix of pMT-SuntagRLucDD-MS2 (200ng), pAWF-MCP-Halotag (5ng), pAWF-scFv-FP (10ng) using effectene transfection reagent. 24h after transfection, cells were first incubated with Schneider's medium containing 200 nM Janelia Fluor® 594 HaloTag® Ligand (Promega GA1110) for 15min and then switched to medium with 1 mM CuSO4 for 1h or 3h to induce expression of pMT construct.

HeLa cells were maintained in DMEM supplemented with 10% FBS, 10 U/ml penicillin/streptomycin and 2.9 mg/ml glutamine in a humidified $CO_2$ incubator at 37°C. For translational inhibition, cells were treated with puromycin at 100 µg/ml for 30 min. Cells were transfected with JetPrime (Polyplus) and selected on 150 µg/ml hygromycin. For each stable cell line, several individual clones were picked and screened by smFISH with sets of fluorescent oligonucleotide probes against the integrated sequence. For CRISPR recombination, clones were additionally analyzed by genomic PCR using amplicons specific for the non-recombined or the recombined allele. The CRISPR guide and repair plasmids have been previously[59]. For the repair plasmid, the 12xALFA-Array replaced the SunTag X56 tag.

The NB-ALFA-sfGFP was introduced into HeLa cells by retroviral infection. HEK293T cells were transiently transfected with a cocktail of plasmids coding for retroviral components and producing the genomic NB-ALFA-sfGFP retroviral RNAs. Viral particles were collected and used to infect recipient HeLa cells, which were then sorted by FACS. Only lowly expressing cells were selected.

**Single molecule fluorescence *in situ* hybridization (smFISH) in mammalian cells**

Cells were grown on glass coverslips (0.17 mm), washed with PBS, fixed in 4% PFA for 20 min, and permeabilized in 70% ethanol overnight at 4°C. Cells were hybridized as previously described[26], except that the probes were sets of unlabeled oligonucleotides hybridizing against the target RNA and additionally contained a common supplementary sequence that was preannealed to a fluorescent oligonucleotide probe termed the FLAP[62]. We used sets of 48 for the DYNC1H1 mRNAs[59]. Slides were mounted in Vectashield with DAPI (Vector Laboratories).

Fixed cells were imaged at room temperature on an Axioimager Z1 wide-field microscope (63×, NA 1.4; ZEISS) equipped with an sCMOs Zyla 4 0.2 camera (Andor Technology) and controlled by MetaMorph (Universal Imaging). 3D image stacks were collected with a Z-spacing of 0.3 µm. Figures were prepared with ImageJ (National Institutes of Health), Photoshop (Adobe Systems), and Illustrator (Adobe Systems)

**Light-Sheet Microscopy**

For light-sheet imaging (related to Movie S6-7 and Figures S1D), the MuViSPIM[63] (Luxendo, Brüker company GMBH) was employed. This setup provides two-sided illumination with two Nikon 10x/0.3 water objectives and two-sided detection with two Olympus 20x/1.0 W objectives. The lightsheet is created by scanning a Gaussian beam, as in digital scanned laser light-sheet microscopy (DSLM). We used the line mode which is an in-built synchronization

between rolling shutter readout mode of sCMOS cameras and digital light sheets canning. This allows the rejection of out-of-focus and scattered light, thus improving the signal to noise ratio. Images are acquired by two ORCA Flash 4.0 (C91440) from Hamamatsu and processed by LuxControl v1.10.2. A 50ms exposure time was used for the green channel with a 488nm laser. Maximum intensity projections were processed with Fiji[64].

**Live imaging of the scFv-FP and NB-ALFA-msGFP2 alone**

For all live imaging experiments, embryos were dechorionated with tape and mounted between a hydrophobic membrane and a coverslip as described previously[65].

Movies for scFv-FP (related to Figure S1 and Movie S1-5) and NB-ALFA-msGFP2 under *nanos* promoter (related to Figure S6 and Movie S23) were acquired using a Zeiss LSM880 confocal microscope with a Plan-Apochromat 40x/1.3 oil objective lens, with green excitation using a 488nm laser (6µw measured with 10x objective lens). A GaAsP detector was used to detect fluorescence with the following settings: 512x 512-pixels images, zoom 2x, each Z-stack comprised of 25 planes spaced 1µm apart.

Movies for *UASp>scFv-FP* (related to Figure S5, and Movie S16-19) and *UASy>scFv-msGFP2* with *nos-Gal4* driver (related to Figure S5 and Movie S21) were acquired using a Zeiss LSM880 confocal microscope with a Plan-Apochromat 40x/1.3 oil objective lens, with green excitation using a 488nm laser (1µw measured with 10x objective lens). A GaAsP detector was used to detect fluorescence with the following settings: 512x 512-pixels images, zoom 2x, each Z-stack comprised of 25 planes spaced 1µm apart.

**Live imaging of the scFv-FP and anti-ALFA-msGFP2 in presence of tagged genes**

For all live imaging experiments, embryos were dechorionated with tape and mounted between a hydrophobic membrane and a coverslip as described previously[65].

Movies of *scFv-FP>twi_suntag_MS2_CRISPR/+* (related to Figure 1 and Movie S8-12) were acquired using a Zeiss LSM880 with confocal microscope in fast Airyscan mode with a Plan-Apochromat 40x/1.3 oil objective lens. GFP was excited using a 488nm (7uw measured with 10x objective lens) laser with the following settings: 132x 132-pixel images, each Z-stack comprised of 15 planes spaced 0.5µm apart and zoom 8x. Intensity measurement of each polysomes was done on a MIP of 5 planes using a custom-made software written in Python, that performs a spot detection on the MIP raw data stack. For each time frame, the software performs a Laplacian of Gaussian 2D filter and the filtered images are than thresholded with a user defined threshold. The threshold is expressed in terms of the average and standard deviation of intensity values of each image in order to have a threshold value self-re-scaled with respect to the characteristic of the images itself. Spots smaller in size than a user-defined value are removed (considered as fake detection). Finally, for each of the detected spots, we use a 2D expansion of the spots silhouettes in order to define a region around the spots devoided of any other spots and that we can use to estimate background and measure it all along the time evolution for corrections purposes.

Movies of *scFv-FP>twi_suntag_MS2_CRISPR/+* and *scFv-msGFP2>twi_suntag_transgene* (related to Figure 2, Figure S4 and Movie S13-15) were acquired using a Zeiss LSM880 with confocal microscope in fast Airyscan mode with a Plan-Apochromat 40x/1.3 oil objective lens. GFP was excited using a 488nm (4.7µW measured with 10x objective lens) laser with the following settings: 568x 568-pixel images, each Z-stack comprised of 61 planes spaced 0.5µm apart and zoom 2x. Movies were then processed to remove frame outside of the embryos or containing the membrane signal to correct drifting, and processed stacks were maximum intensity projected using custom-made software, developed in Python™[7].

Movies of *nos-Gal4>UASp-scFv-msGFP2* x *twi_suntag_MS2_CRISPR/+* and *scFv-msGFP2* x *twi_suntag_MS2_CRISPR/+* (related to Figure 3 and Movie S20) were acquired using a Zeiss

674 LSM880 with confocal microscope in fast Airyscan mode with a Plan-Apochromat 40x/1.3 oil
675 objective lens. GFP was excited using a 488nm (5uw measure with 10x objective lens) laser
676 with the following settings: 396x 396-pixel images, each Z-stack comprised of 30 planes spaced
677 0.5µm apart and zoom 4x.
678 Live tilescans of *nullo-Gal4*>UASy-*scFv-msGFP2-NLS* (related to Movie S22) were acquired
679 using a Zeiss LSM880 with confocal microscope in fast Airyscan mode with a Plan-
680 Apochromat 40x/1.3 oil objective lens. GFP was excited using a 488nm (13µW measured with
681 10x objective lens) laser with the following settings: 1440 x 2746-pixel images using two tiles,
682 each Z-stack comprised of 9 planes spaced 2µm apart and zoom 0.8x.
683 Live tilescans of *UASy-scFv-msGFP2-NLS/ his2Av-RFP* in presence or not of *nullo-Gal4* driver
684 (related to Supplementary Figure S5E) were acquired using a Zeiss LSM880 with confocal
685 microscope in fast Airyscan mode with a Plan-Apochromat 40x/1.3 oil objective lens. GFP was
686 excited using a 488nm (13µW measured with 10x objective lens) and RFP was excited using a
687 561nm laser with the following settings: 1024 x 3072-pixel images using three tiles, each Z-
688 stack comprised of 14 planes spaced 2µm apart.
689 Movies of NB-ALFA-msGFP2 under *nanos* EPr crossed with *Ilp4_32x_ALFA-array* (related
690 to Figure 4 and Movie S24) were acquired using a Zeiss LSM880 with confocal microscope in
691 fast Airyscan mode with a Plan-Apochromat 40x/1.3 oil objective lens. GFP was excited using
692 a 488nm (6.4µW measured with 10x objective lens) laser with the following settings: 256x 256-
693 pixel images, each Z-stack comprised of 6 planes spaced 1µm apart and zoom 6x.
694 Live tilescans of NB-ALFA-msGFP2 under *nanos* EPr crossed with *Ilp4_32x_ALFA-array*
695 (related to Figure S6 and Movie S25) were acquired using a Zeiss LSM880 with confocal
696 microscope in fast Airyscan mode with a Plan-Apochromat 40x/1.3 oil objective lens. GFP was
697 excited using a 488nm (13µW measured with 10x objective lens) laser with the following
698 settings: 1612 x 4860-pixel images using 3 tiles, each Z-stack comprised of 9 planes spaced
699 2µm apart.
700
701 **S2 cell culture imaging:**
702 Cells were pipetted into a µ-Slide (Ibidi #80621) and live-imaged using a Zeiss LSM980
703 confocal microscope with an Airyscan detector in SR mode with a 63X Plan-Apochromat
704 (1.4NA) oil objective lens. GFP was excited using a 488nm laser and MCP-Halotag labelled by
705 Janelia Fluor® 594 was excited using a 561nm laser. Cells with mRNAs visible in cytoplasm
706 and with comparable GFP signal were chosen for acquiring images. Images of individual cells
707 were acquired with following setting: z-stack of 5 planes with 0.5um interval, 8x zoom,
708 396x396 pixel and 8 bit per pixel. GFP foci co-localized with mRNA foci (Janelia Fluor® 594
709 signal) were considered as translation sites while GFP foci or larger amorphous or ring-like
710 GFP structures that were not co-localized with mRNA were considered as aggregates.
711
712
713 **References:**
714 1. Pichon, X. *et al.* Visualization of single endogenous polysomes reveals the dynamics of
715 translation in live human cells. *J Cell Biol* **214**, 769–781 (2016).
716 2. Wang, C., Han, B., Zhou, R. & Zhuang, X. Real-Time Imaging of Translation on
717 Single mRNA Transcripts in Live Cells. *Cell* **165**, 990–1001 (2016).
718 3. Morisaki, T. *et al.* Real-time quantification of single RNA translation dynamics in
719 living cells. *Science (1979)* **352**, 1425–1429 (2016).
720 4. Wu, B., Eliscovich, C., Yoon, Y. J. & Singer, R. H. Translation dynamics of single
721 mRNAs in live cells and neurons. *Science (1979)* **352**, 1430–1435 (2016).
722 5. Yan, X., Hoek, T. A., Vale, R. D. & Tanenbaum, M. E. Dynamics of Translation of
723 Single mRNA Molecules In Vivo. *Cell* **165**, 976–989 (2016).

6. Formicola, N. *et al.* Tyramine induces dynamic RNP granule remodeling and translation activation in the Drosophila brain. *Elife* **10**, (2021).
7. Dufourt, J. *et al.* Imaging translation dynamics in live embryos reveals spatial heterogeneities. *Science (1979)* **372**, 840–844 (2021).
8. Vinter, D. J., Hoppe, C., Minchington, T. G., Sutcliffe, C. & Ashe, H. L. Dynamics of hunchback translation in real-time and at single-mRNA resolution in the Drosophila embryo. *Development* **148**, (2021).
9. Lecerf, J.-M. *et al.* Human single-chain Fv intrabodies counteract *in situ* huntingtin aggregation in cellular models of Huntington's disease. *Proceedings of the National Academy of Sciences* **98**, 4764–4769 (2001).
10. Wörn, A. *et al.* Correlation between in vitro stability and in vivo performance of anti-GCN4 intrabodies as cytoplasmic inhibitors. *J Biol Chem* **275**, 2795–2803 (2000).
11. Colby, D. W. *et al.* Development of a human light chain variable domain (V(L)) intracellular antibody specific for the amino terminus of huntingtin via yeast surface display. *J Mol Biol* **342**, 901–912 (2004).
12. Tanenbaum, M. E., Gilbert, L. A., Qi, L. S., Weissman, J. S. & Vale, R. D. A protein-tagging system for signal amplification in gene expression and fluorescence imaging. *Cell* **159**, 635–646 (2014).
13. Chouaib, R. *et al.* A Dual Protein-mRNA Localization Screen Reveals Compartmentalized Translation and Widespread Co-translational RNA Targeting. *Dev Cell* **54**, 773-791.e5 (2020).
14. Boersma, S. *et al.* Translation and Replication Dynamics of Single RNA Viruses. *Cell* **183**, 1930-1945.e23 (2020).
15. Bruurs, L. J. M. *et al.* Heterogeneity in viral replication dynamics shapes the antiviral response. *bioRxiv* 2022.06.08.495262 (2022) doi:10.1101/2022.06.08.495262.
16. Boersma, S. *et al.* Multi-Color Single-Molecule Imaging Uncovers Extensive Heterogeneity in mRNA Decoding. *Cell* **178**, 458-472 e19 (2019).
17. Safieddine, A. *et al.* A choreography of centrosomal mRNAs reveals a conserved localization mechanism involving active polysome transport. *Nat Commun* **12**, 1352 (2021).
18. Chalfie, M., Tu, Y., Euskirchen, G., Ward, W. W. & Prasher, D. C. Green fluorescent protein as a marker for gene expression. *Science* **263**, 802–805 (1994).
19. Prasher, D. C., Eckenrode, V. K., Ward, W. W., Prendergast, F. G. & Cormier, M. J. Primary structure of the Aequorea victoria green-fluorescent protein. *Gene* **111**, 229–233 (1992).
20. Zacharias, D. A., Violin, J. D., Newton, A. C. & Tsien, R. Y. Partitioning of lipid-modified monomeric GFPs into membrane microdomains of live cells. *Science (1979)* **296**, (2002).
21. Rodriguez, E. A. *et al.* The Growing and Glowing Toolbox of Fluorescent and Photoactive Proteins. *Trends Biochem Sci* **42**, 111–129 (2017).
22. Lambert, G. G. *et al.* Aequorea's secrets revealed: New fluorescent proteins with unique properties for bioimaging and biosensing. *PLoS Biol* **18**, (2020).
23. Bindels, D. S. *et al.* mScarlet: a bright monomeric red fluorescent protein for cellular imaging. *Nat Methods* **14**, 53–56 (2017).
24. Leake, M. C. & Quinn, S. D. A guide to small fluorescent probes for single-molecule biophysics. *Chemical Physics Reviews* **4**, 011302 (2023).
25. Bertrand, E. *et al.* Localization of ASH1 mRNA particles in living yeast. *Mol Cell* **2**, 437–445 (1998).

26. Fusco, D. *et al. Single mRNA Molecules Demonstrate Probabilistic Movement in Living Mammalian Cells HHS Public Access Author manuscript*. *Curr Biol* vol. 13 http://images.cellpress.com/supmat/supmatin.htm. (2003).
27. Forrest, K. M. & Gavis, E. R. Live imaging of endogenous RNA reveals a diffusion and entrapment mechanism for nanos mRNA localization in Drosophila. *Curr Biol* **13**, 1159–1168 (2003).
28. Tantale, K. *et al.* A single-molecule view of transcription reveals convoys of RNA polymerases and multi-scale bursting. *Nat Commun* (2016) doi:10.1038/ncomms12248.
29. Dufourt, J. *et al.* Imaging translation dynamics in live embryos reveals spatial heterogeneities. *Science (1979)* **372**, 840–844 (2021).
30. Tutucci, E. *et al.* An improved MS2 system for accurate reporting of the mRNA life cycle. *Nat Methods* **15**, 81–89 (2018).
31. Hocine, S., Raymond, P., Zenklusen, D., Chao, J. A. & Singer, R. H. Single-molecule analysis of gene expression using two-color RNA labeling in live yeast. *Nat Methods* **10**, 119–121 (2013).
32. Weil, T. T., Parton, R. M. & Davis, I. Making the message clear: visualizing mRNA localization. *Trends Cell Biol* **20**, 380–390 (2010).
33. Tutucci, E. *et al.* An improved MS2 system for accurate reporting of the mRNA life cycle. *Nat Methods* **15**, 81–89 (2018).
34. Pichon, X., Robert, M.-C., Bertrand, E., Singer, R. H. & Tutucci, E. New Generations of MS2 Variants and MCP Fusions to Detect Single mRNAs in Living Eukaryotic Cells. *Methods Mol Biol* **2166**, 121–144 (2020).
35. Tanenbaum, M. E., Gilbert, L. A., Qi, L. S., Weissman, J. S. & Vale, R. D. A protein-tagging system for signal amplification in gene expression and fluorescence imaging. *Cell* **159**, 635–646 (2014).
36. Wörn, A. *et al.* Correlation between in vitro stability and in vivo performance of anti-GCN4 intrabodies as cytoplasmic inhibitors. *J Biol Chem* **275**, 2795–2803 (2000).
37. Donahue, C. E. T., Siroky, M. D. & White, K. A. An Optogenetic Tool to Raise Intracellular pH in Single Cells and Drive Localized Membrane Dynamics. *J Am Chem Soc* **143**, (2021).
38. Chen, D. & McKearin, D. M. A discrete transcriptional silencer in the bam gene determines asymmetric division of the Drosophila germline stem cell. *Development* **130**, 1159–1170 (2003).
39. Ali, I. *et al.* Cis-regulatory elements affecting the Nanos gene promoter in the germline stem cells. *J Biotechnol* **145**, 323–329 (2010).
40. Doren, M. Van, Williamson, A. L. & Lehmann, R. Regulation of zygotic gene expression in Drosophila primordial germ cells. *Current Biology* **8**, 243–246 (1998).
41. Garcia, H. G., Tikhonov, M., Lin, A. & Gregor, T. Quantitative Imaging of Transcription in Living Drosophila Embryos Links Polymerase Activity to Patterning. *Current Biology* (2013) doi:10.1016/j.cub.2013.08.054.
42. Pédelacq, J. D., Cabantous, S., Tran, T., Terwilliger, T. C. & Waldo, G. S. Engineering and characterization of a superfolder green fluorescent protein. *Nat Biotechnol* **24**, (2006).
43. Valbuena, F. M. *et al.* A photostable monomeric superfolder green fluorescent protein. *Traffic* **21**, (2020).
44. Campbell, B. C. *et al.* mGreenLantern: a bright monomeric fluorescent protein with rapid expression and cell filling properties for neuronal imaging. *Proc Natl Acad Sci U S A* **117**, (2020).
45. Shaner, N. C. *et al.* A bright monomeric green fluorescent protein derived from Branchiostoma lanceolatum. *Nat Methods* **10**, (2013).

46. Pan, D. J., Huang, J. D. & Courey, A. J. Functional analysis of the Drosophila twist promoter reveals a dorsal-binding ventral activator region. *Genes Dev* **5**, 1892–1901 (1991).
47. Brogiolo, W. *et al.* An evolutionarily conserved function of the drosophila insulin receptor and insulin-like peptides in growth control. *Current Biology* **11**, (2001).
48. Vinter, D. J., Hoppe, C., Minchington, T. G., Sutcliffe, C. & Ashe, H. L. Dynamics of hunchback translation in real-time and at single-mRNA resolution in the Drosophila embryo. *Development* **148**, (2021).
49. Rørth, P. Gal4 in the Drosophila female germline. *Mech Dev* **78**, 113–118 (1998).
50. Brand, A. H. & Perrimon, N. Targeted gene expression as a means of altering cell fates and generating dominant phenotypes. *Development* **118**, 401–415 (1993).
51. DeLuca, S. Z. & Spradling, A. C. Efficient Expression of Genes in the Drosophila Germline Using a UAS Promoter Free of Interference by Hsp70 piRNAs. *Genetics* **209**, 381–387 (2018).
52. Götzke, H. *et al.* The ALFA-tag is a highly versatile tool for nanobody-based bioscience applications. *Nat Commun* **10**, 4403 (2019).
53. Alessandra Vigano, M. *et al.* Protein manipulation using single copies of short peptide tags in cultured cells and in Drosophila melanogaster. *Development (Cambridge)* **148**, (2021).
54. Song, S.-J., Diao, H.-P., Moon, B., Yun, A. & Hwang, I. The B1 Domain of Streptococcal Protein G Serves as a Multi-Functional Tag for Recombinant Protein Production in Plants. *Front Plant Sci* **13**, (2022).
55. Bothma, J. P., Norstad, M. R., Alamos, S. & Garcia, H. G. LlamaTags: A Versatile Tool to Image Transcription Factor Dynamics in Live Embryos. *Cell* **173**, 1810-1822.e16 (2018).
56. Mateju, D. *et al.* Single-Molecule Imaging Reveals Translation of mRNAs Localized to Stress Granules. *Cell* **183**, 1801-1812.e13 (2020).
57. Ramat, A. *et al.* The PIWI protein Aubergine recruits eIF3 to activate translation in the germ plasm. *Cell Res* **30**, 421–435 (2020).
58. Kang, J.-Y. *et al.* LLPS of FXR1 drives spermiogenesis by activating translation of stored mRNAs. *Science (1979)* **377**, eabj6647 (2022).
59. Pichon, X. *et al.* Visualization of single endogenous polysomes reveals the dynamics of translation in live human cells. *J Cell Biol* **214**, 769–781 (2016).
60. Venken, K. J. T., He, Y., Hoskins, R. A. & Bellen, H. J. P[acman]: A BAC transgenic platform for targeted insertion of large DNA fragments in D. melanogaster. *Science (1979)* **314**, 1747–1751 (2006).
61. Tantale, K. *et al.* Stochastic pausing at latent HIV-1 promoters generates transcriptional bursting. *Nat Commun* **12**, 4503 (2021).
62. Tsanov, N. *et al.* SmiFISH and FISH-quant - A flexible single RNA detection approach with super-resolution capability. *Nucleic Acids Res* **44**, (2016).
63. Krzic, U., Gunther, S., Saunders, T. E., Streichan, S. J. & Hufnagel, L. Multiview light-sheet microscope for rapid in toto imaging. *Nat Methods* **9**, 730–733 (2012).
64. Schindelin, J. *et al.* Fiji: an open-source platform for biological-image analysis. *Nat Methods* **9**, 676–682 (2012).
65. Dufourt, J. *et al.* Temporal control of gene expression by the pioneer factor Zelda through transient interactions in hubs. *Nat Commun* **9**, (2018).

**Acknowledgments:**

We are grateful to NanoTag Biotechnologies for sharing ALFA-Tag and anti-ALFA nanobody plasmids and advices. We are grateful to Karim Mazjoub's lab for sharing space in his experimental room. We thank Drs. Xavier Pichon and Vera Slaninova for their help in setting up the mammalian ALFA-Tag system. For imaging, we acknowledge Sylvain de Rossi and Montpellier Ressources Imagerie (MRI), a microscopy facility of The National Infrastructure France-BioImaging (FBI), supported by the French National Research Agency (ANR-10-INBS-04). We acknowledge M.Verbrugghe for help with fly handling, and the Montpellier *Drosophila* Facility (BioCampus). We acknowledge Etienne Schwob and Eric Kremer for their help in preparing the manuscript. We acknowledge HFSP (CDA Grant to ML) for the early sponsoring of the implementation of *Drosophila* translation imaging project.

**Funding:** This work was supported by the ERC SyncDev starting grant to ML, the ANR MemoRNP to ML, and by IGMM internal capital. ML, JD, EB and CF are sponsored by CNRS. MB was supported by a FRM fellowship and then by ERC SyncDev. HL was supported by ERC SyncDev. JDh was supported by ANR grant ULTIM.

**Author contributions:** JD conceived the project. JD conceptually supervised the work with the help of ML at its early stages. JD, MB, ML, EB, RL and RC designed the experiments. JD, MB, and CF performed *Drosophila* embryos experiments. AT developed software. HL helped with cloning and fly handling. ML acquired funding. EB supervised mammalian cells experiments, which were performed by JDh. RL supervised *Drosophila* S2 cells experiments performed by RC. JD, MB, RC, AT, EB and CF analyzed and interpreted the results. JD and MB wrote the manuscript. ML, RC, EB, RL and CF edited the manuscript. All authors discussed and approved the manuscript.

**Competing interests:** The authors declare that they have no competing interests.

**Data and materials availability:** All relevant data supporting the key findings of this study are available within the article and its Supplementary Information files or from the corresponding author upon reasonable request. The intensity measurement software is available through this link: https://github.com/ant-trullo/Av_Ints_software/. Fly lines and plasmids will be available upon peer-reviewed publication of the article.

## Supplementary figures

Figure S1

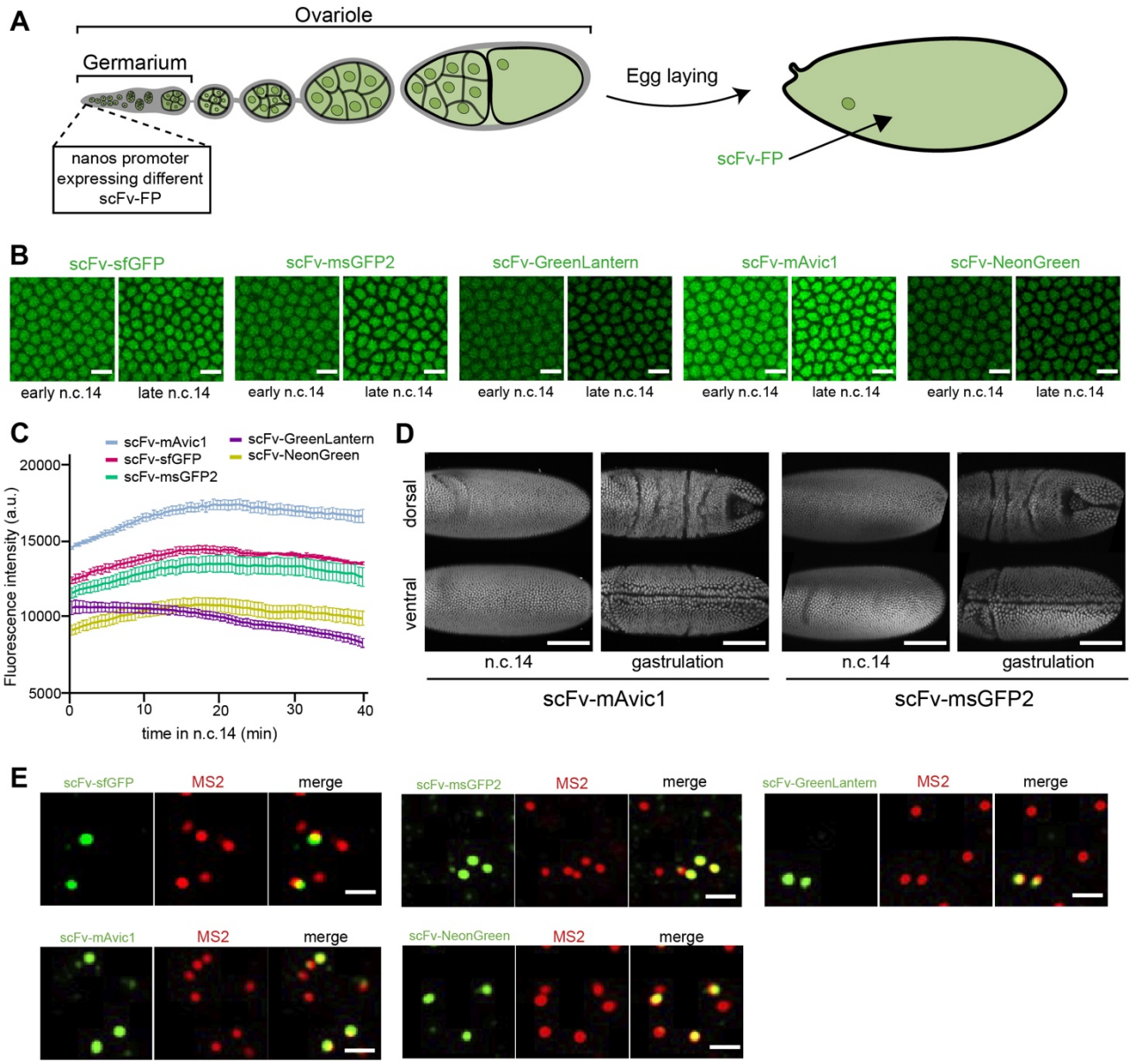


**Figure Supp 1: Characterization of the different scFv-Fluorescent proteins (scFv-FP).**
(**A**) Schematic of the expression pattern of scFv-FP under control of the *nanos* enhancer/promoter during *Drosophila* oogenesis. (**B**) Snapshots from movies on embryos carrying scFv-sfGFP, scFv-msGFP2, scFv-GreenLantern, scFv-mAvic1 or scFv-NeonGreen in early and late n.c. 14. Scale bars are 10µm. (see related Movies S1-5). (**C**) Quantification across time during n.c. 14 of the different scFv-FP signal from movies represented in (b), n=3 movies from 3 embryos for scFv-sfGFP and scFv-GreenLantern and n=4 movies from 4 embryos for scFv-msGFP2, scFv-mAvic1 and scFv-NeonGreen. Error bars represent SEM. (**D**) Snapshots from light-sheet movies on embryos carrying scFv-mAvic1 or scFv-msGFP2 in n.c. 14 and at gastrulation stage. Ventral and dorsal view are represented for each embryo. Scale bars are 100µm. (See related Movies S6-7). (**E**) Single Z-planes of confocal images from smFISH with direct fluorescent protein signal in green (scFv-msGFP2, scFv-GreenLantern, scFv-mAvic1, scFv-NeonGreen and scFv-sfGFP) and *MS2* probes (red) on *scFv-FP x twi_suntag_MS2_CRISPR* embryos in early-mid n.c. 14 on the ventral side. Images represent zoomed images from Figure 1c. Scale bars are 1µm.

Figure S2

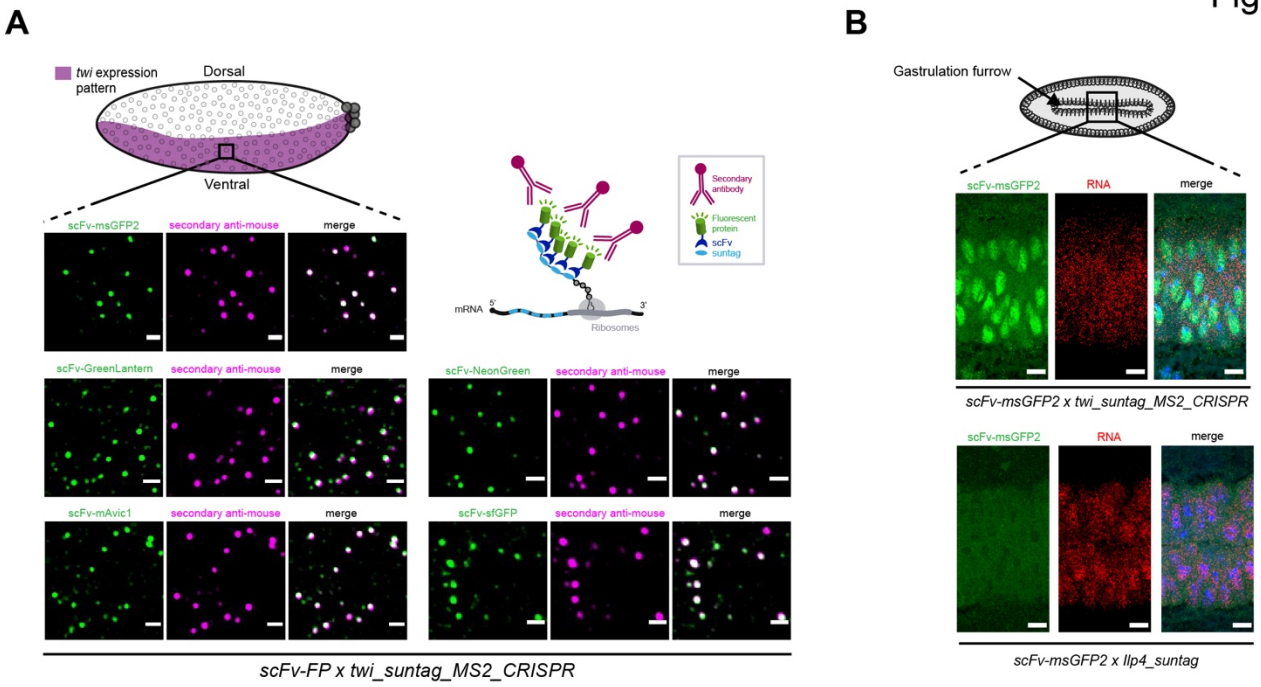


**Figure Supp 2: Localization of the tagged protein and scFv recognition by secondary antibody.**
(**A**) (top) Schematic of a sagittal view of a *Drosophila* embryo with *twi* expression pattern in purple. Black square represents the imaged area of the bottom panels. Single Z-planes of confocal images from immuno-staining with direct fluorescent protein signal in green (scFv-msGFP2, scFv-GreenLantern, scFv-mAvic1, scFv-NeonGreen and scFv-sfGFP) and secondary anti-mouse antibody (magenta) on *scFv-FP x twi_suntag_MS2_CRISPR* embryos in n.c. 14 on the ventral side. Note the co-localization between the direct fluorescent protein signal and the secondary antibody signal as illustrated by the schematic on the top right. Scale bar are 1µm. (**B**) (top) Schematic of a *Drosophila* embryo on the ventral side with gastrulation furrow represented with invaginating cells. Black square represents the imaged area of the bottom panels. (bottom) Single Z-planes of confocal images from smFISH with direct scFv-msGFP2 fluorescent protein signal (green) and *MS2* or *Ilp4* probes (red) on *scFv-msGFP2 > twi_suntag_MS2_CRISPR* and *scFv-msGFP2 > Ilp4_suntag* embryos at gastrulation stage and on the ventral side. Note a nuclear signal in *twi_suntag_trangene* embryos and a cytoplasmic signal in *Ilp4_suntag* embryos. Scale bars are 10µm.

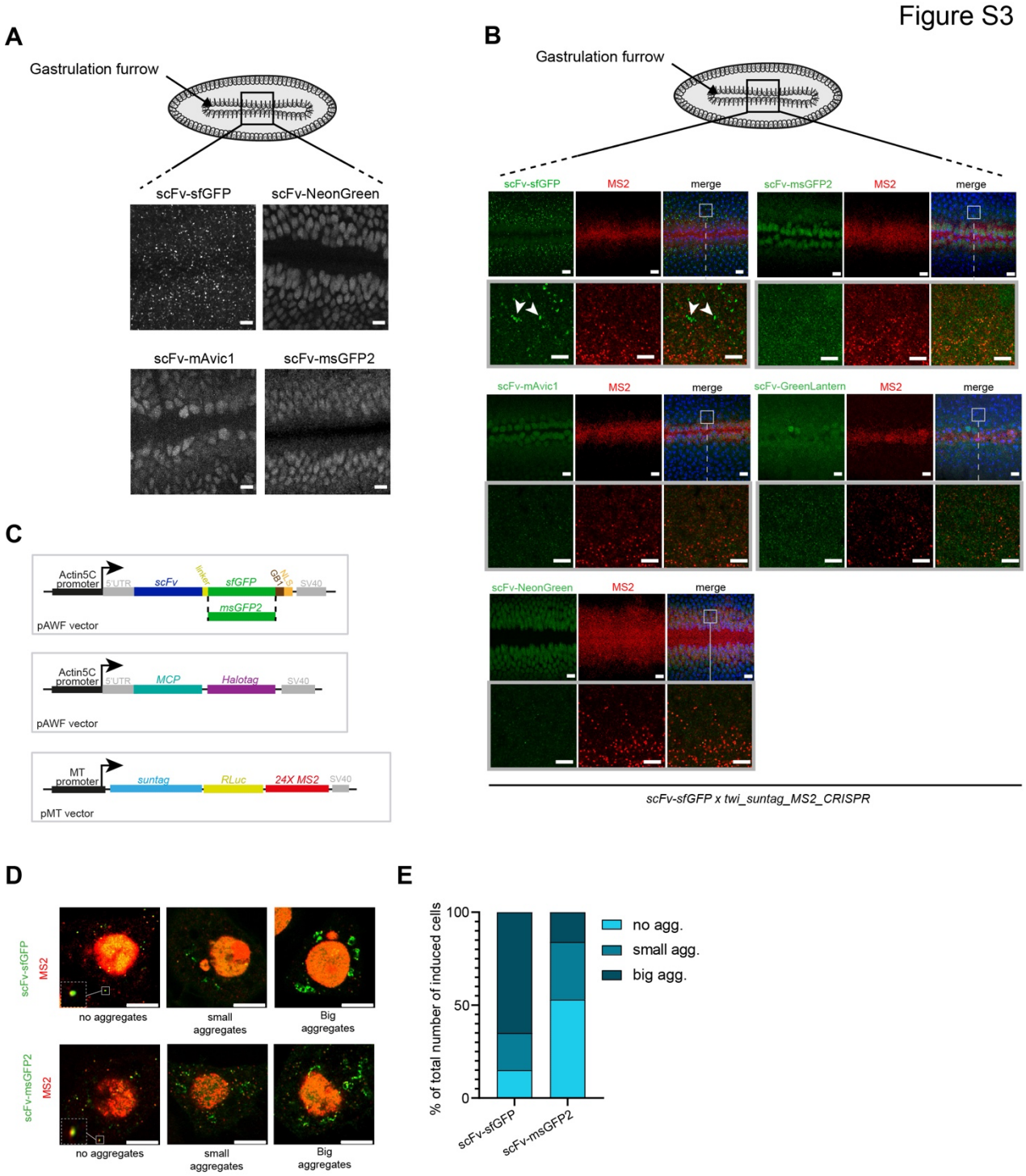


**Figure Supp 3: The scFv-sfGFP can form aggregates in *Drosophila* embryos and S2 cells**
(**A**) Schematic of a *Drosophila* embryo on the ventral side with gastrulation furrow represented with invaginating cells. Black square represents the imaged area of the bottom panels. Snapshots from representative confocal movies of *twi_suntag_MS2_CRISPR/+* embryos at the gastrulation stage carrying either scFv-sfGFP, scFv-NeonGreen, scFv-mAvic1 or scFv-msGFP2 proteins. Scale bars are 10µm. (**B**) Schematic of a *Drosophila* embryo on the ventral side with gastrulation furrow represented with invaginating cells. Black square represents the imaged area of the bottom panels. Maximum intensity projection of 10 Z-planes of confocal images from smFISH with direct fluorescent protein signal in green (scFv-FP) and *MS2* probes (red) on *scFv-FP x twi_suntag_MS2_CRISPR* embryos at gastrulation stage on the ventral side. Grey squares represent zoomed images. Note the presence of scFv-sfGFP signal not overlapping with RNA (white arrowheads). Scale bars are 5µm. (**C**) Schematic of the different constructs transfected in S2 cells. *scFv-FPs* and *tdMCP-stdHalotag* were

placed downstream of the *Actin5C* promoter. Reporter containing suntag Renilla Luciferase (RLuc) and 24XMS2 was placed under the control of the inducible metallothionein (MT) promoter. (**D**) Single Z-planes of confocal images of S2 cells expressing scFv-FPs (green) and MCP-Halotag (red) with induction of *suntagRLuc24XMS2* reporter showing aggregation size of the scFv-FPs. A zoom on single mRNA in translation is shown on no aggregate's panels (white squares). Scale bars are 5µm. **e.** Percentage of the number of big (dark blue) and small (blue) aggregates (scFv-FP signal not colocalizing with an mRNA) and no (light blue) aggregates (scFv-FP signal colocalizing with an mRNA) in cells expressing *MCP-Halotag*, *suntagRLuc24XMS2* reporter and *scFv-sfGFP2* or *scFv-msGFP2* (n=100 cells for each condition).

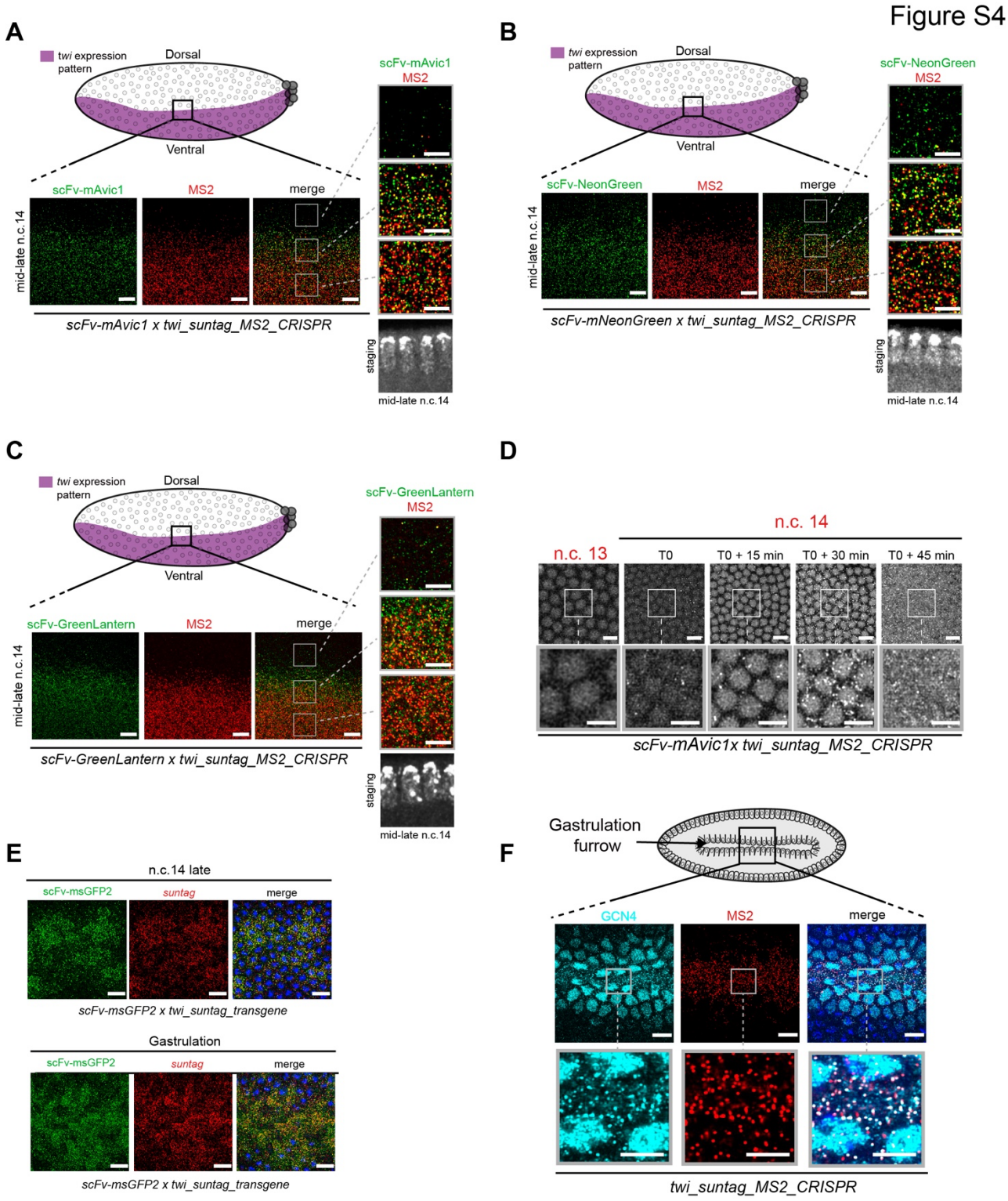


**Figure Supp 4: *twi* translation detection in developing embryos until gastrulation.**
(**A**) (top) Schematic of a sagittal view of a *Drosophila* embryo with *twi* expression pattern in purple. Anterior side is on the left, posterior on the right, dorsal on the top and ventral side on the bottom. Black square represents the imaged area of the bottom panels. (bottom) A single Z-plane of confocal images from smFISH with direct fluorescent protein signal in green (scFv-mAvic1) and *MS2* probes (red) on *scFv-mAvic1 x twi_suntag_MS2_CRISPR* embryos at mid-late n.c. 14. Gray squares represent the zoomed images in the right panels. The three different zoomed images represent external (top), border (middle) and internal (bottom) zone of the imaged pattern. Scale bars are 10µm on the larger images, and 5µm on the zoomed images. Staging is given

by DAPI staining on a sagittal view of the imaged embryo (black and white image at the bottom). (**B**) (top) Schematic of a sagittal view of a *Drosophila* embryo with *twi* expression pattern in purple. Anterior side is on the left, posterior on the right, dorsal on the top and ventral side on the bottom. Black square represents the imaged area of the bottom panels. (bottom) A single Z-plane of confocal images from smFISH with direct fluorescent protein signal in green (scFv-NeonGreen) and *MS2* probes (red) on *scFv-NeonGreen x twi_suntag_MS2_CRISPR* embryos at mid-late n.c. 14. Gray squares represent the zoomed images in the right panels. The three different zoomed images represent external (top), border (middle) and internal (bottom) zone of the imaged pattern. Scale bars are 10µm on the larger images, and 5µm on the zoomed images. Staging is given by DAPI staining on a sagittal view of the imaged embryo (black and white image at the bottom). (**C**) (top) Schematic of a sagittal view of a *Drosophila* embryo with *twi* expression pattern in purple. Anterior side is on the left, posterior on the right, dorsal on the top and ventral side on the bottom. Black square represents the imaged area of the bottom panels. (bottom) A single Z-plane of confocal images from smFISH with direct fluorescent protein signal in green (scFv-GreenLantern) and *MS2* probes (red) on *scFv-GreenLantern x twi_suntag_MS2_CRISPR* embryos at mid-late n.c. 14. Gray squares represent the zoomed images in the right panels. The three different zoomed images represent external (top), border (middle) and internal (bottom) zone of the imaged pattern. Scale bars are 10µm on the larger images, and 5µm on the zoomed images. Staging is given by DAPI staining on a sagittal view of the imaged embryo (black and white image at the bottom). (**D**) Snapshots each 15 minutes from movies of *scFv-msGFP2 x twi_suntag_MS2_CRISPR* embryos on the ventral side. T0 correspond to early n.c.14. White squares represent the zoomed images in the center of the panel. Note the absence of translation for *twi_suntag_MS2_CRISPR* at T0+45min, Scale bars are 10µm on the larger images, and 5µm on the zoomed images. (See related Movies S15). **e.** Single Z-planes of confocal images from smFISH with direct fluorescent protein signal in green (scFv-msGFP2) and *suntag* probes (red) on *scFv-msGFP2 x twi_suntag_transgene* embryos in late n.c. 14 (top panels) and gastrulation stage (bottom panels) on the ventral side. Nuclei are counterstained with DAPI (blue). Scale bars are 10µm. **f.** (top) Schematic of a *Drosophila* embryo on the ventral side with gastrulation furrow represented with invaginating cells. Black square represents the imaged area of the bottom panels. (bottom) Single Z-planes of confocal images from immuno-smFISH with anti-GCN4 antibody (cyan) and MS2 probes (red) on *twi_suntag_MS2_CRISPR* embryos. Grey squares represent the zoomed images in the bottom panels. Scale bars are 10µm on the larger images, and 5µm on the zoomed images.

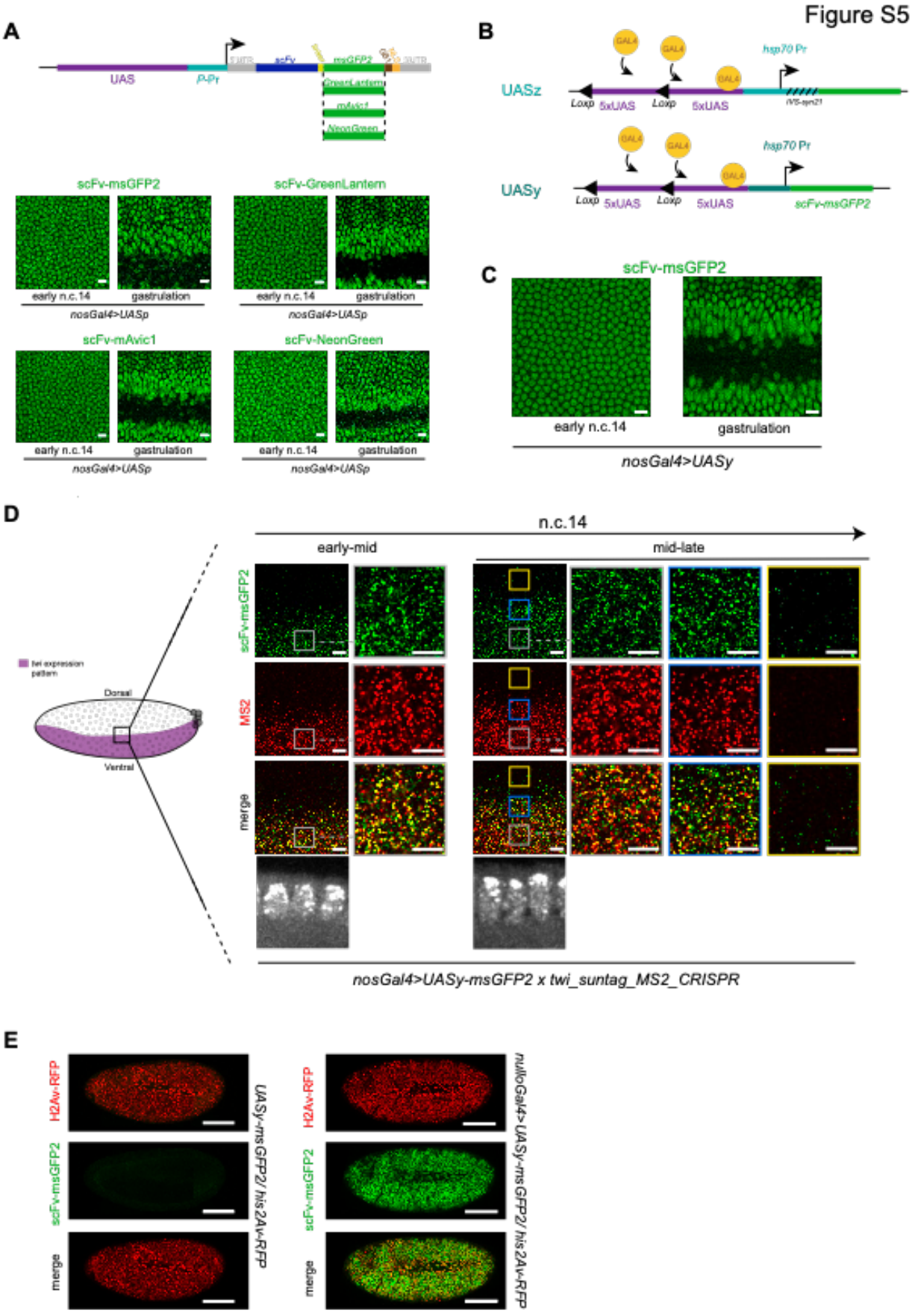


**Figure Supp 5: Generation of UAS-Gal4 system to express scFv-Fluorescent Proteins**

(**A**) (top) Schematic of the different constructs expressing the different scFv-FP (scFv-GreenLantern, scFv-NeonGreen, scFv-mAvic1, or scFv-msGFP2) under the control of the UASp promoter. (bottom) Snapshots from movies of embryos carrying *UASp-scFv-msGFP2, UASp-scFv-GreenLantern, UASp-scFv-mAvic1* or *UASp-scFv-NeonGreen* and *nanos-Gal4* at early n.c.14 and gastrulation stage. Scale bars are 10µm. (See related Movies S16-19). (**B**) Schematic of the two constructs UASz and UASy containing two times *5xUAS* with *hsp70* promoter with *IVS-syn21* sequence (UASz) or without (UASy). Both of these constructs contain the *scFv-msGFP2*. (**C**) Snapshots from movies of embryos carrying *UASy-scFv-msGFP2* and *nanos-Gal4* at early n.c.14 and gastrulation stage. Scale bars are 5µm. (See related Movies S21). (**D**) (left) Schematic of a sagittal view of a *Drosophila* embryo with *twi* expression pattern in purple. Anterior side is on the left, posterior on the right, dorsal on the top and ventral side on the bottom. Black square represents the imaged area of the right panels. (right) A single Z-plane of confocal images from smFISH with direct fluorescent protein signal in green (scFv-msGFP2) and *MS2* probes (red) on *nosGal4>UASy-scFv-msGFP2 x twi_suntag_MS2_CRISPR* embryos in early-mid and mid-late n.c. 14. Staging is given by DAPI staining on a sagittal view of the embryo (black and white image at the bottom). Yellow, blue and white squares (external, border and internal zone of the pattern, respectively) represent the three different zoomed images on the right side of each panel. Scale bars are 10µm on the larger images, and 5µm on the zoomed images. (**E**) Maximum intensity projected snapshots of a whole embryos confocal live tilescan expressing *UASy-scFv-msGFP2* and *Histone-H2A-RFP* (left panels) or *nulloGal4>UASy-scFv-msGFP2 and Histone-H2A-RFP* (right panels), after gastrulation. Scale bars are 100µm.

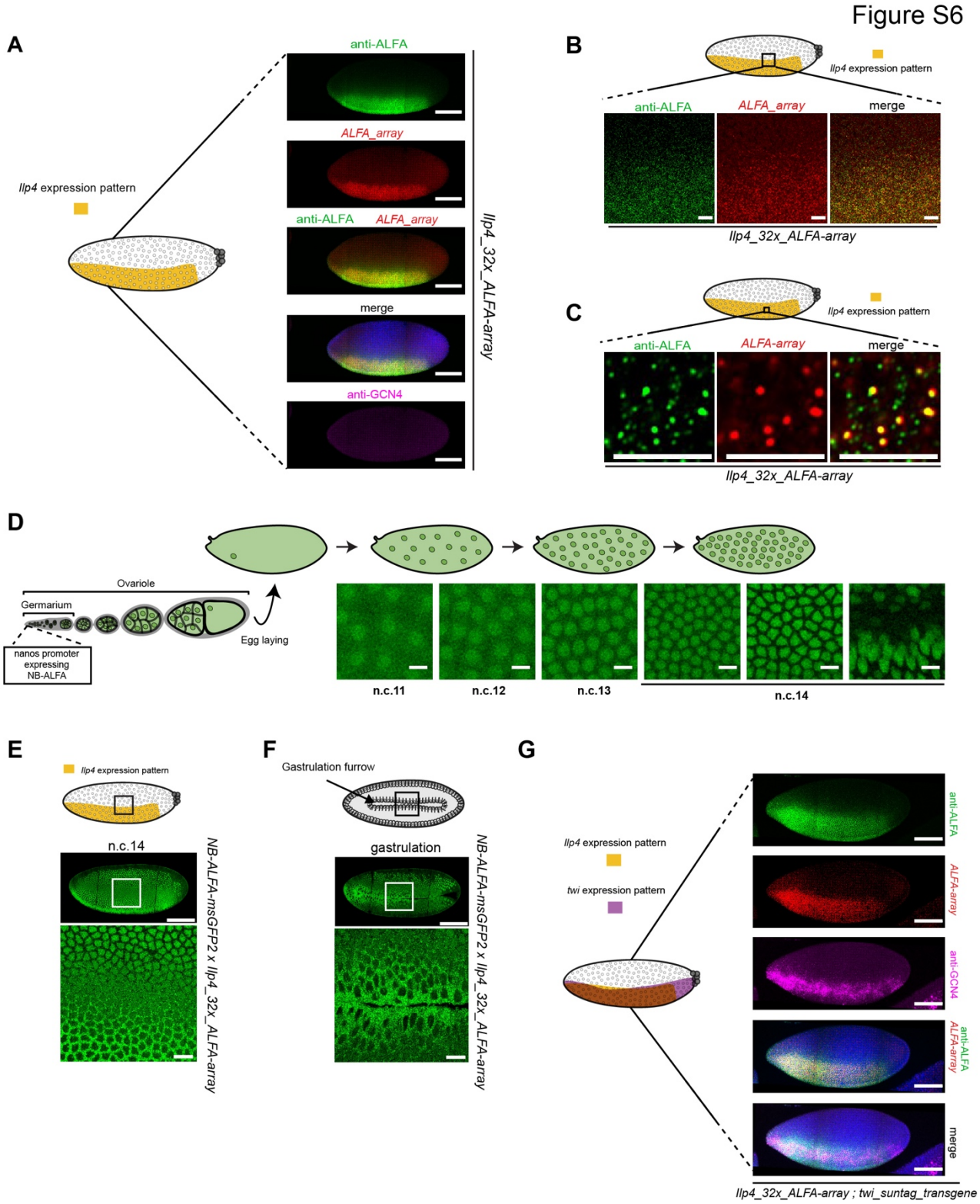


**Figure Supp 6: Efficient detection of *Ilp4* transgene translation with the new AlfaTag system**
(**A**) (left) Schematic of a sagittal view of a *Drosophila* embryo with *Ilp4* expression pattern in yellow. Anterior side is on the left, posterior on the right, dorsal on the top and ventral side on the bottom. (right) Maximum intensity projection of a whole embryo tilescan confocal images from immuno-smFISH with anti-ALFA antibody (green), *32x_ALFA-array* probes (red) and anti-GCN4 antibody (magenta) on *Ilp4_32x_ALFA-array* n.c.14 embryos. Scale bars are 100µm. (**B**) (top) Schematic of a sagittal view of a *Drosophila* embryo with *Ilp4* expression pattern in yellow. Black square represents the imaged area of the bottom panels. (bottom) Single Z-planes of confocal images from immuno-smFISH with anti-ALFA antibody (green) and *32x_ALFA-array* probes

(red) on *Ilp4_32x_ALFA-array* in early-mid n.c. 14 embryos at the border of *Ilp4* expression pattern. Scale bars are 10µm. (**C**) (top) Schematic of a sagittal view of a *Drosophila* embryo with *Ilp4* expression pattern in yellow. Black square represents the imaged area of the bottom panels. (bottom) Single Z-planes of confocal images from immuno-smFISH with anti-ALFA antibody (green) and *32x_ALFA-array* probes (red) on *Ilp4_32x_ALFA-array* in early-mid n.c. 14 embryos to visualize single mRNA molecules in translation. Scale bars are 5µm. (**D**) (top) Schematic of the expression pattern of NB-ALFA under control of the *nos EPr* during *Drosophila* oogenesis. (bottom) Snapshots from movies of embryos carrying *nos>NB-ALFA-msGFP2* in n.c. 11, 12, 13 and 14. Scale bars are 10µm. (See related Movies S23). (**E**) (top) Schematic of a sagittal view of a *Drosophila* embryo with *Ilp4* expression pattern in yellow. Black square represents the imaged area of the bottom panel. (bottom) Snapshots from movies of *NB-ALFA-msGFP2 x Ilp4_32x_ALFA-array* embryos in n.c. 14. The top image is a tile scan of the whole embryo and the bottom image a zoomed area represented with a white square at the border of *Ilp4* expression pattern. Note the green signal located in nuclei outside the pattern and in the cytoplasm within *Ilp4* pattern (corresponding to tagged Ilp4 proteins). Scale bars are 100µm in the tilescan and 10µm in the zoomed image. (See related Movies S25). (**F**) (top) Schematic of a sagittal view of a *Drosophila* embryo with *Ilp4* expression pattern in yellow. Black square represents the imaged area of the bottom panel. (bottom) Snapshots from movies of *NB-ALFA_msGFP2 > Ilp4_32x_ALFA-array* embryos at gastrulation stage. The top image is a tile scan of the whole embryo and the bottom image a zoomed area represented with a white square at the gastrulation furrow. Scale bars are 100µm in the tilescan and 10µm in the zoomed image. (See related Movies S24). (**G**) Maximum intensity projection of a whole embryo tilescan confocal images from immuno-smFISH with anti-ALFA antibody (green), *32x_ALFA-array* probes (red) and anti-GCN4 antibody (magenta) on *Ilp4_32x_ALFA-array; twi_suntag_transgene* embryos in n.c. 14. Scale bars are 100µm.

## Movie Supp legends

**Movie S1**: Maximum intensity projection of confocal Z-stack live imaging of an embryo containing *scFv-sfGFP*. scale bar 10µm.
**Movie S2**: Maximum intensity projection of confocal Z-stack live imaging of an embryo containing *scFv-mAvic1*. scale bar 10µm.
**Movie S3**: Maximum intensity projection of confocal Z-stack live imaging of an embryo containing *scFv-msGFP2*. scale bar 10µm.
**Movie S4**: Maximum intensity projection of confocal Z-stack live imaging of an embryo containing *scFv-NeonGreen*. scale bar 10µm.
**Movie S5**: Maximum intensity projection of confocal Z-stack live imaging of an embryo containing *scFv-GreenLantern*. scale bar 10µm.
**Movie S6**: Maximum intensity projection of LightSheet Z-stack live imaging of *scFv-mAvic1* embryo. Upper part: dorsal view, lower part: ventral view Scale bar 100µm.
**Movie S7**: Maximum intensity projection of LightSheet Z-stack live imaging of *scFv-msGFP2* embryo. Upper part: dorsal view, lower part: ventral view Scale bar 100µm.
**Movie S8**: Maximum intensity projection of confocal Z-stack fast live imaging of an embryo containing *scFv-NeonGreen>twi_suntag_MS2_CRISPR/+*. Translation foci are in green, scale bar 1µm.
**Movie S9**: Maximum intensity projection of confocal Z-stack fast live imaging of an embryo containing *scFv-sfGFP >twi_suntag_MS2_CRISPR/+*. Translation foci are in green, scale bar 1µm.
**Movie S10**: Maximum intensity projection of confocal Z-stack fast live imaging of an embryo containing *scFv-GreenLantern >twi_suntag_MS2_CRISPR/+*. Translation foci are in green, scale bar 1µm.
**Movie S11**: Maximum intensity projection of confocal Z-stack fast live imaging of an embryo containing *scFv-msGFP2>twi_suntag_MS2_CRISPR/+*. Translation foci are in green, scale bar 1µm.
**Movie S12**: Maximum intensity projection of confocal Z-stack fast live imaging of an embryo containing *scFv-mAvic1>twi_suntag_MS2_CRISPR/+*. Translation foci are in green, scale bar 1µm.

**Movie S13**: Maximum intensity projection of confocal Z-stack live imaging of an embryo containing *scFv-msGFP2>twi_suntag_MS2_CRISPR/+*. Translation foci are in white, scale bar 10µm.
**Movie S14**: Maximum intensity projection of confocal Z-stack live imaging of an embryo containing *scFv-msGFP2>twi_suntag_transgene/+*. Translation foci are in white, scale bar 10µm.
**Movie S15**: Maximum intensity projection of confocal Z-stack live imaging of an embryo containing *scFv-mAvic1> twi_suntag_transgene/+*. Translation foci are in white, scale bar 10µm.
**Movie S16**: Maximum intensity projection of confocal Z-stack live imaging of an embryo containing *nos-Gal4>UASp-scFv-GreenLantern /+*. scale bar 10µm.
**Movie S17**: Maximum intensity projection of confocal Z-stack live imaging of an embryo containing *nos-Gal4>UASp-scFv-msGFP2 /+*. scale bar 10µm.
**Movie S18**: Maximum intensity projection of confocal Z-stack live imaging of an embryo containing *nos-Gal4>UASp-scFv-NeonGreen /+*. scale bar 10µm.
**Movie S19**: Maximum intensity projection of confocal Z-stack live imaging of an embryo containing *nos-Gal4>UASp-scFv-mAvic1 /+*. scale bar 10µm.
**Movie S20**: Comparison of maximum intensity projection of confocal Z-stack live imaging of an embryo containing *scFv-msGFP2>twi_suntag_MS2_CRISPR/+ or nos-Gal4>UASp-scFv-mAvic1 ; twi_suntag_MS2_CRISPR/+*. Translation foci are in white. Translationnal arrest is seen *scFv-msGFP2>twi_suntag_MS2_CRISPR/+ but not* in *nos-Gal4>UASp-scFv-mAvic1 ; twi_suntag_MS2_CRISPR/+*. scale bar 10µm.
**Movie S21**: Maximum intensity projection of confocal Z-stack live imaging of an embryo containing *nos-Gal4>UASy-scFv-msGFP2 /+*. scale bar 10µm.
**Movie S22**: Maximum intensity projection of confocal Z-stack live imaging of an embryo containing *nullo-Gal4>UASy-scFv-msGFP2 /+*. scale bar 100µm.
**Movie S23**: Maximum intensity projection of confocal Z-stack live imaging of an embryo containing *NB-ALFA-msGFP2*. scale bar 10µm.
**Movie S24**: Maximum intensity projection of confocal Z-stack live imaging of an embryo containing *NB-ALFA-msGFP2> Ilp4_32x_ALFA-array/+*. Scale bar 10µm.
**Movie S25**: Maximum intensity projection of confocal tile-scan with Z-stack live imaging of an embryo containing *NB-ALFA-msGFP2> Ilp4_32x_ALFA-array/+*. Scale bar 100µm.